TOSHKENT DAVLAT TRANSPORT UNIVERSITETI
Tashkent state transport university
International Journal Of Transport And Technological Machines
Tashkent 2024, issue 1, https://ijttm.uz/

TOSHKENT DAVLAT TRANSPORT UNIVERSITETI
Tashkent state transport university

Issue 1, 2024

INTERNATIONAL JOURNAL OF TRANSPORT AND TECHNOLOGICAL MACHINES

ISSN: 3030-363X



THE SCIENCE OF TODAY IS THE TECHNOLOGY OF TOMORROW

INTERNATIONAL JOURNAL OF TRANSPORT AND TECHNOLOGICAL MACHINES

Published since 2023

Editorial Council:
Mukhitdinov A.A., Ziyayev K.Z., Rustamov K.J, Abdurazzakov U.
Editorial team:
Chief Editor – Rustamova N.R.
Deputy Chief Editor – Rustamov K.J.

Members of the editorial board:
Mukhitdinov A.A., Ziyayev K.Z., Rustamov K.J., Abdurazzoqov U.A., Saman M. Almufti., Habibollah Haron., Gai-ge Wang., Jayson A. Dela Fuente., Ahmad A. AlRabab'ah., Rami Hikmat Fouad AL-Hadeethi., Emad Kamil Hussein., Ayman Abu-Rumman.

TASHKENT STATE TRANSPORT UNIVERSITY

Founder of the scientific and technical journal, “International Journal of Transport and Technological Machines” – Tashkent State Transport University (100167, Republic of Uzbekistan, Tashkent, Temiryulchilar str., house No. 1, office: 379, tel Tel.: +998 97 156 94 21 E-mail: k.j.rustamov82@gmail.com).

In the International Journal of Transport and Technological Machines publishes the most significant results of scientific and applied research carried out in universities of transport and information technology profile, other higher educational institutions, research institutes and centers of the Republic of Uzbekistan and foreign countries.

The journal is published 4 times a year and contains publications in the following main areas:

- Automotive engineering
- Civil Engineering
- Construction Engineering and Management
- Instrumentation technology
- Environmental Engineering
- Environmental Sciences
- Green production
- Industrial Safety
- Mechanical Engineering Technology
- Mining
- Mechatronics

CONTENTS

1. Akhmedov D., Riskaliev D. OPTIMIZATION RATIONAL PARAMETERS OF THE DRIVING SIMULATOR..... 4
2. Valiev J., Avliyokulov J., Gangfeng Tanb. TO STUDY THE FACTORS INFLUENCING THE EFFICIENCY OF SUCTION OF DUST PARTICLES WITH THE REGENERATIVE AIR VACUUM SWEEPER PICK-UP HEAD..... 10
3. Kapskya D.V., Mukhitdinov A.A. REDUCING THE DANGER OF PASSING CONFLICTS IN TRAFFIC FLOW AT CONTROLLED INTERSECTIONS USING VEHICLE DETECTORS…… 21
4. Maksudov Z.T., Rustamov K.J., Pardabaev Z.A. STUDY OF PERFORMANCE INDICATORS OF EXCAVATORS…….. 30

TOSHKENT DAVLAT TRANSPORT UNIVERSITETI
Tashkent state transport university
International Journal Of Transport And Technological Machines
Tashkent 2024, issue 1, https://ijttm.uz/

OPTIMIZATION RATIONAL PARAMETERS OF THE DRIVING SIMULATOR

Doniyor Akhmedov [1], Davron Riskaliev [2]

[1] Public Safety University of the Republic of Uzbekistan, Tashkent, Uzbekistan

[2] Tashkent State Transport University, Tashkent, Uzbekistan

[b] *Corresponding author: davron.riskalievsh@tstu.uz*

Abstract: This study aims to achieve accurate simulation alignment with real-life road conditions for optimal training effectiveness. By investigating the tilt and displacement of the vehicle during manoeuvres, experiments establish a basis for configuring simulation parameters. The goal is to attain correlation with empirical observations and adjust the simulator's rational parameters accordingly. The study's specific aim is to determine these parameters and locate the optimal installation coordinates for the electric motor within the simulator structure.

Key words: simulator, adaptation, manoeuvres, rational parameters, electric motor, crankshaft and motion reducer.

Introduction

Optimising rational parameters in driving simulators is a critical pursuit that is essential for enhancing their efficacy in various applications, including driver training, research, and development. In order to improve the adaptation of the simulated scenarios displayed on the simulator monitor to the real road conditions, it is essential to elicit an appropriate response from the simulator [1,2,7,8]. For example, whilst performing manoeuvres on various routes, like ascending an overpass, the lorry adjusts its orientation with an angle α (Figure 1). Experimental studies have determined the values of tilt and displacement of the car on different paths [3,4,5]. In order to reproduce such phenomena, the rational parameters of the simulation have to be adapted to those derived from experimental data.

The aim of this study is to determine the rational parameters of the simulator and the installation coordinates of the electric motor. The main components of the simulator are shown in Figure 2. As shown, the electric motor (5) is connected to the worm gearbox (6). The crankshaft (1) is securely fixed to the shaft of the worm gear reducer by means of a key. The upper surfaces of the crankshaft (2) act as a connecting rod and are supported by means of ball bearings and a screw assembly. The upper part of the P-shaped upper surface accommodates a spherical bearing hinge (3), which is connected to the upper part by bolted ears and secured by a bolt. This hinge is in turn connected to the central platform (4) by a

finger. This finger is mounted by a bolt. When activated, the simulator transmits motion from the engine to the motion reducer, causing the crankshaft (1) to rotate at a maximum speed of 1800 rpm. The P-shaped upper surface, which acts as a connecting rod, induces a complex movement in the crankshaft, which results in vertical oscillations or reciprocating movements in the central platform (4). The electronic frequency of the reducer of the electric motor is modulated in order to vary the frequency of the torque and the stop occurs when the upper part (2) of the crankshaft reaches its zenith (at 1800 revolutions).

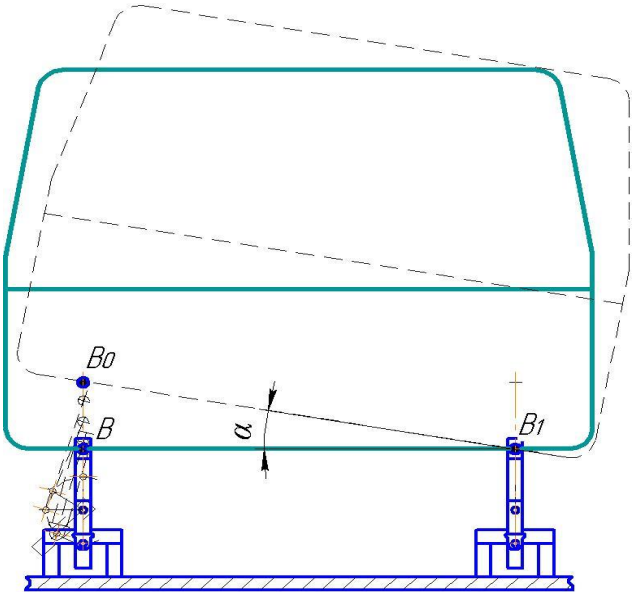


Figure 1. The pitch (rolling) of the simulator cabin due to the movement of the motion components.

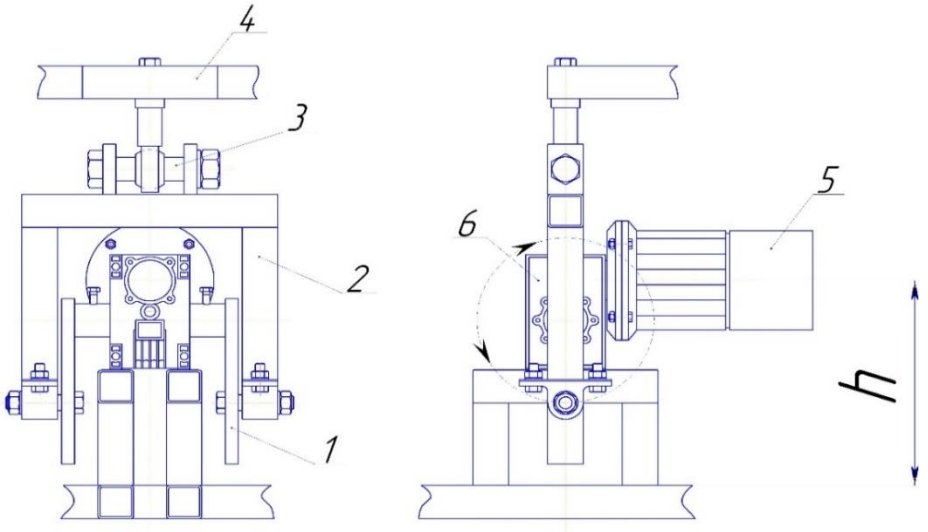


Figure 2. Main components of the simulator: 1-crankshaft; 2-simulator upper part (connecting rod); 3-simulator hinge bushing; 4-central platform; 5-electric motor; 6-worm gear reducer; h-height of installing the electric motor on the frame.

Using the calculation diagram shown in Figure 3, the dimensions of the crankshaft, the length of the simulator's upper part (connecting rod) and the installation coordinates of the electric motor are determined, thus determining the basic kinematic and geometric parameters of the simulator mechanism. One of the main objectives is to identify rational simulator movement parameters. When the simulator cabin is moving at its maximum inclination (Figure 3), it is necessary to take into account the angle of cabin inclination (α = 10-120) and to minimise the load on points A and B of the simulator movement in order to select the appropriate parameters for the simulator. These are indispensable factors to be taken into account.

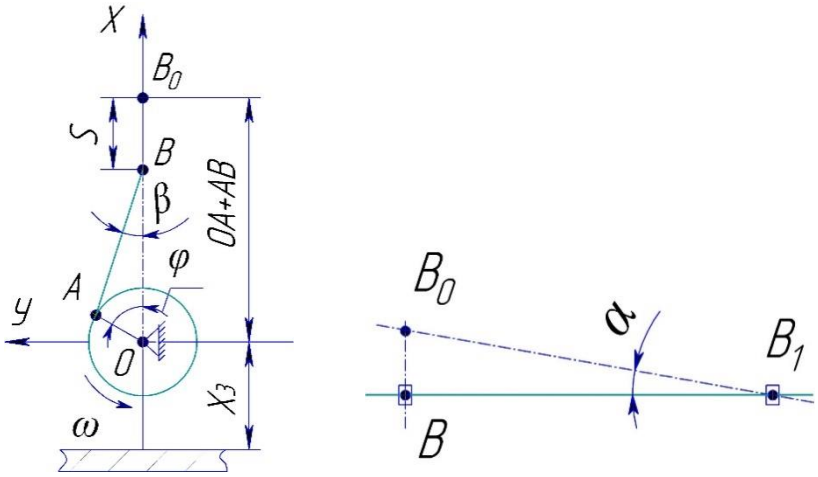


Figure 3. Computational diagram for determining the rational parameters of the simulator motion.

The following information can be derived from the above calculation diagram:

$$OB = OA\cos\varphi + AB\cos\beta = OA + OB. \quad (1)$$

According to the Law of Sines:

$$\frac{OA}{\sin\beta} = \frac{AB}{\sin\varphi} \quad (2)$$

$$\sin\beta = \frac{OA}{AB}\sin\varphi$$

from this point,

$$\cos\beta = \sqrt{1-(\frac{OA}{AB})^2\sin^2\varphi} \quad (3)$$

The chassis displacement along the S-axis during the complete cycle of crankshaft movement is calculated as follows:

$$S = OA(1-\cos\varphi) + AB(1-\sqrt{1-(\frac{OA}{AB})^2 \sin^2\varphi} \quad (4)$$

In the course of the chassis displacement along the S distance in the motion of the mechanism, the inclination (roll), denoted as α, of the body with respect to the BB_0B_1 plane is observed. This is in accordance with the Law of Sines, and it is expressed as follows [2]:

$$\frac{BB_0}{\sin\alpha} = \frac{B_0B_1}{\sin(90-\frac{\alpha}{2})} = \frac{B_0B_1}{\sqrt{\frac{1+\cos\alpha}{2}}}, \quad (5)$$

$$\frac{\sqrt{\frac{1+\cos\alpha}{2}}}{\sin\alpha} = \frac{B_0B_1}{B_0B_1}. \quad (6)$$

From the Law of Cosines:

$$BB_0^2 = B_0B_1^2 + BB_1^2 - 2B_0B_1 \cdot BB_1\cos\alpha. \quad (7)$$

from this point,

$$\cos\alpha = \frac{BB_0^2 + BB_1^2 - B_0B_1^2}{2B_0B_1 \cdot BB_1\cos\alpha} \quad (8)$$

Subsequently, the velocity magnitudes at points A and B are calculated:

$$v_A = \sqrt{v_{xA}^2 + v_{yA}^2}, \; v_B = \sqrt{v_{yA}^2 + v_{yB}^2} \quad (9)$$

$$v_{xA} = -OA\omega\sin\varphi, \; v_{yA} = -OA\omega\cos\varphi \quad (10)$$

Here, ω represents the angular velocity of the worm gear reducer.

The velocities at points A and B are calculated as follows:

$$a_A = \sqrt{v_{xA}^2 + v_{yA}^2}, \; a_B = \sqrt{v_{yA}^2 + v_{yB}^2} \quad (11)$$

$$a_{xA} = -OA\omega^2\cos\varphi, \; a_{yA} = -OA\omega^2\sin\varphi \quad (12)$$

On the basis of the above, it is essential to determine the installation coordinates and acceptable lengths for the simulator to simulate the tilt of the body as closely as possible to the actual circumstances and to reduce the applied load. To facilitate this process, experimental methods were utilised [3]. The following independent factors were considered as characteristics:

– X_1: Length of the crankshaft used in the simulator, measured in millimetres (mm).

– X_2: Length of the upper section of the simulator's connecting rod, measured in millimetres.
– X_3: Height for the installation of the electric motor onto the frame, measured in millimetres.

Table 1 displays the levels of the factors and the extent of their variations.

Table 1. Values of Factor Levels and Ranges of Change for the Factors

Indicator	*Factor* X_1		*Factor* X_2		*Factor* X_3	
	Actual Value, mm	Encoded Value	Actual Value, mm	Encoded Value	Actual Value, mm	Encoded Value
Variation Range	15	–	30	–	20	–
Upper Level	150	+1	380	+1	320	+1
Baseline Level	135	0	350	0	300	0
Lower Level	120	-1	320	-1	280	-1

Drawing upon the acquired experimental outcomes, the rational parameters of the simulator mechanism have been discerned and empirically validated. The findings indicate that the most suitable parameters for the designed simulator encompass a crankshaft length between 120 and 125 millimeters, an upper part (connecting rod) length ranging from 350 to 365 millimeters, and an optimal height for the installation of the electric motor on the frame within the span of 300 to 315 millimeters.

Conclusion.

In conclusion, this study has presented an exhaustive analysis focused on optimizing the rational parameters of driving simulators, crucial for enhancing their effectiveness in various domains such as driver training and automotive engineering. By conducting empirical inquiries, the research has scrupulously scrutinized the tilt and displacement of vehicles during maneuvers to establish associations with real-world road conditions, thus setting the foundation for configuring simulation parameters.

The results emphasize the utmost importance of faithfully replicating vehicle dynamics within the simulator setting. Through determining the most suitable parameters for the simulator mechanism, which includes the crankshaft length (ranging between 120 and 125 millimeters), the upper part length of the connecting rod (ranging from 350 to 365 millimeters), and the installation height of the electric motor on the frame (falling within the

range of 300 to 315 millimeters), the study aims to reduce stress on simulator components while optimizing simulation accuracy.

References

1. D.A. Akhmedov, Alimuxamedov Sh.P., Narziev S.O., Modeling the influence of the steering wheel by the driver on the vehicle motion. Construction Mechanics, Hydraulics and Water Resources. E3S Web of Conferences 264, 05015 (2021) CONMECHYDRO-2021. https://doi.org/10.1051./e3sconf/202126405015.

2. D.A. Akhmedov, B.A. Aliboev. Kinematic Optimization of the Steering and Suspension Systems of a Modernized Car // ISNN 1068-798X, Russian Engineering Research, 2021, Vol. 41, No. 6, pp. 484-488. © Allerton Press, Inc., 2021. Russian Text © The Author(s), 2021, published in Vestnik Mashinostroeniya, 2021, No3, pp. 21-24.

3. Адлер Ю.П. Введение в планирование экспериментов: учеб. пособие. – М.: Изд. Дом МИСиС, 2014.- 36 с.

4. L. Sung, K. Ha, C. H. Cho, and L. J. Lee, “The KOOKMIN University Driving Simulators for Vehicle Control System Development and Human Factor Study,” in Driving Simulation Conference (DSC04), Paris, France, 2015.

5. Кравченко Л.А., Дубинина Ж.В., Берека И.А. Система обучения водителей в автошколе с учетом личностных качеств // Вестник Московского автомобильно-дорожного государственного технического университета (МАДИ). 2019. № 1 (56). С. 42–48.

6. Calvi A., Benedetto A., De Blasiis M.R. A driving simulator study of driver performance on deceleration lanes // Accident Analysis and Prevention. 2017 т. 45. С. 195–203.

7. Ikehaga S., “Active Suspension Control of Ground Vehicle based on a Full-Vehicle Model”, American Control Conference, pp.4019-4024, 2000.

8. Guo L, Ge PS, Yue M, et al. Lane changing trajectory planning and tracking controller design for intelligent vehicle running on curved road. Math Probl Eng 2014; 2014: 1–9

TOSHKENT DAVLAT TRANSPORT UNIVERSITETI
Tashkent state transport university
International Journal Of Transport And Technological Machines
Tashkent 2024, issue 1, https://ijttm.uz/

TO STUDY THE FACTORS INFLUENCING THE EFFICIENCY OF SUCTION OF DUST PARTICLES WITH THE REGENERATIVE AIR VACUUM SWEEPER PICK-UP HEAD

Jamshid Valiev[1)], Avliyokulov Jamshed[a], Gangfeng Tan[2)]

[1)]Tashkent State Transport University, Tashkent, Uzbekistan

[2)]Wuhan University of Technology, Wuhan, China

Corresponding author: jams.Valiev@mail.ru

Abstract This paper is about a numerical measurement of the factors affecting the efficiency of removal of debris and particles on the road surface by the suction head of a regenerative sweeper. Based on particle removal starting speed, particle throughput, particle removal efficiency, and experimental results. A proven computational fluid dynamics model is proposed to evaluate the removal efficiency of particles moving through the suction channel with the direction of airflow movement of the designed regenerative air-vacuum sweeper pick-up head. The factors affecting the efficiency of waste and particle collection were evaluated by developing an experimental setup for a regenerative air suction system. The numerical simulation and experimental results show that the particle structure, sweeping speed, the distance between the suction channel and road surface, and pressure drop at the head of the sweeper strongly affect the particle removal efficiency. The particle removal efficiency increases when the particle mass is lighter, the sweeping speed is lower, the suction mouth channel is closer to the road surface, the airflow in the inlet channels creates a lower negative pressure around the suction mouth, the higher the density, the smaller the particle suction mouth, and the higher the efficiency when the airflow is increased. In addition, data are obtained to increase the efficiency of particle collection by the pickup head of the regenerative air vacuum sweeper.

Key words: ANSYS CFD, Environment, Dust and particles, Urban street cleaning, lifting devices, general suction.

Introduction

The deterioration of environmental conditions leads to pollution from natural disasters or sandstorms in various cities. To reduce the impact of dust and particles on human health, it is important to keep the environment and city streets clean. Always keep city streets clean to prevent the spread of dust and particles in the city during high winds, to prevent the accumulation of mud on the road surface and water supply systems during incessant rain, serves to prevent urban pollution. In large cities, many manpower and technologies are used to clean the streets, all of which leads to high costs [1, 2]. The use of high-efficiency regenerative air cleaners in cleaning urban streets helps to prevent the spread of dust and particles into the environment and effectively clean the street waste[3]. The sweeping suction head is an important part of the regenerative air vacuum sweeper, which picks-up dust and particles and returns the airflow in the system [4]. There are a large number of particles and debris on the road surface. Highly efficient suction of any kind of waste is very important for regenerative air vacuum road sweepers.

Much research has been conducted to evaluate and improve the effectiveness of cleaning roads of particles and debris. For example, Wu et al[5, 6] analyzed the factors affecting the efficiency of particle removal. It was found that changes in particle size and sweeper speed had a significant effect on suction performance during the numerical study. Zhang and others [7] analyzed the effects of changes in the structure and composition of particles and debris on the initial velocity of particles. They pointed out that it is possible to increase efficiency by optimizing the blower system of the sweeper. Structural changes in particles lead to an increase in mass, which in turn can affect the suction power of the sweeper [8]. In the process of changing the particle structure, it is possible to increase the efficiency of particle assimilation by changing the airflow rate and pressure of the different inlet ducts in the centrifugal blower [9]. Xi et al[10] analyzed the efficiency of particle assimilation by changing the size of the inlet port. Xi et al [11] the importance of air pressure in the suction mouth by analyzing the characteristics of particle movement is discussed in

detail in the collection of waste and debris. Daichin et al [12] analyzed the improvement of the vacuum cleaner by developing and modifying the suction head by conducting experiments to ensure good dust and particle collection.

This study took into account the assessment of factors influencing the efficiency of suction of dust and particles of the regenerative air vacuum sweeper pick-up head. The effect of the distance between the collection head and the road surface on the efficiency of particle collection. Theoretical calculation of the effect of particle assimilation efficiency on the initial velocity of particles and the effect of pressure change on the assimilation efficiency, the creation of a simulation model of the trajectory variability of airflow in the inlet and suction mouth. The high efficiency of particle removal was optimized using the experimental method of a single design by conducting a simulation analysis of the flow field at different variable lifting and gravitational forces, taking into consideration the preliminary design parameters of the project.

Experimental Set-up

As shown in Fig.1, 3D models are a regenerative air vacuum sweeper system experiment-set-up. The regenerative air sweeper pickup head plays an important role in clearing dust and particles from the road. In the newly designed pick-up head model, factors influencing the suction efficiency of dust and particles are observed. The pick-up head has a conventional suction mouth and two inlet channels to receive the airflow returning from the system. Pick-up head suction mouth diameter can be changed. The suction mouth with a diameter of 100mm to 140mm is employed for the experiment. The pick-up head input channels use smaller inlet ducts with a diameter of 60mm to 100mm. The CY200H centrifugal fan begins to suck up dust and particles on the surface of the conveyor belt by generating high-pressure airflow through the pick-up head suction mouth during the operation. The particles absorbed through the dust and absorption mouth are taken to the dust collecting hopper and the airflow continues to move through the filter after it is separated from the particles. The airflow inside the pick-up head suction duct is between 5 m/s and 35 m/s where the centrifugal fan airflow rate-regulated is performed by the AC inverter frequency drive SQ580-011G / 015P-4. In order to observe how dust and particles affect the assimilation efficiency when the distance between the pick-up head and the converter belt changes. The Hiudon SWL 2.5T is fitted with special lifting devices. These devices allow the pick-up head to move up and down, at an angle of 30° to the right and left sides. Using a conveyor belt, the movement of dust and particles is done. The conveyor speed can get up to 40 km/h. There is a special control device to adjust the speed of the conveyor belt, the effect of the change in particle velocity on the suction efficiency by changing the conveyor speed is considered. A dust feeder with a control mechanism was implemented on the conveyor belt to ensure the even distribution of dust and particles. Particles of size PM10 to 120 mm can be distributed through the dust feeder.

The regenerative air sweeper pick-up head was designed using the ANSYS CFD program to calculate the factors influencing the suction efficiency by determining the trajectory of the airflow through the suction and inlet channels.

1. Study the direction of a particle flow motion by observing the particle trajectory in the pick-up head suction channel
2. Observation of airflow direction and factors influencing an airflow and the particle movement through the pick-up head inlet channels
3. Increase the absorption efficiency of suction dust and particles by detecting the movement of an environment airflow towards the suction channel.

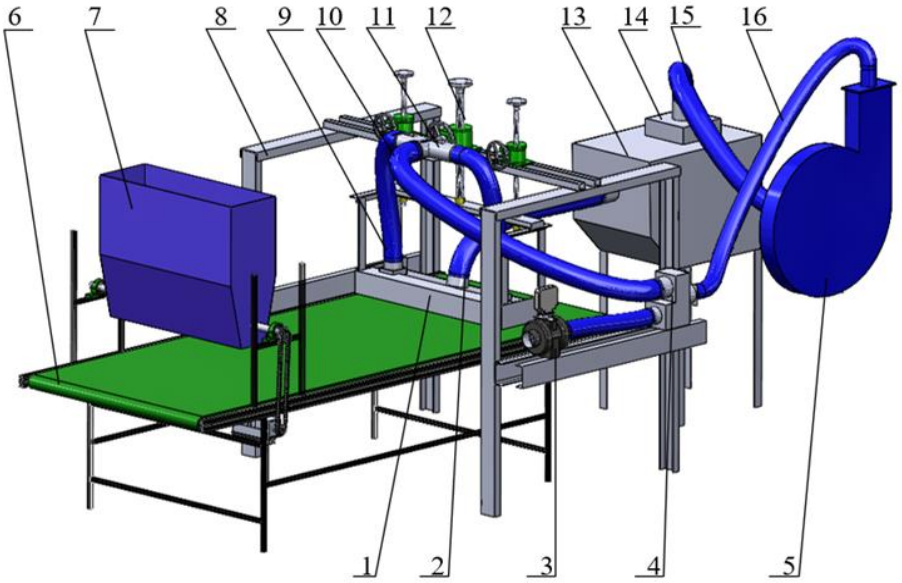


Fig 2. 3D model regenerative air vacuum sweeper system experiment-set-up Simulation
1-Pick-up head; 2-Suction mouth; 3-Electronic control valve; 4-Air separation box; 5-Centrifugal fan; 6-Conveyer belt; 7-Dust feeder; 8-Frame base; 9-Inlet mouth; 10- Blowing inlet duct; 11-Mechanical valve; 12-Lifting device; 13-Dust collector hopper; 14-Filter place; 15-Cenctrigugal fan inlet duct; 16-centrifugal fan outlet duct

Structure parameters of dust collection pick-up head

Typically, regenerative air sweepers, the pick-up head must usually ensure complete circulation of the airflow in the system. The pick-up head must ensure that the airflow from the system is returned to the system along with the extraction of debris and particles on the road surface. In many cases, an effective method for determining the assimilation performance efficiency of the pick-up head is to analyze the simulation results of this designed pick-up head using a program CFD. Mesh creation in computational fluid dynamics (CFD) plays an important role in increasing the accuracy and efficiency of numerical simulation. In order to achieve high efficiency, in the first stage of the CFD program, a brief understanding of the improved reception head model can be obtained by determining the airflow trajectory in the inlet and outlet ducts. The preliminary data of the pick-up head can be shown in Table 1, and the pick-up head physical model in Fig. 2.

Table 1. The main dimensions of the regenerative air sweeper pick-up head

Length (mm)	*Width (mm)*	*Height (mm)*	*Thickness (mm)*	*Outlet duct D1(mm)*	*Inlet duct D2(mm)*	*Inlet duct D3(mm)*
1000	*390*	*120*	*20*	*110*	*65*	*65*

The airflow through the regenerative air vacuum cleaning system was calculated using governing equations. Although the airflow was turbulent at high Reynolds numbers, it was not a strong rotational flow. Airflow trajectories can be simulated by means of CFD software using corresponding mathematical models of flow field conditions such as trace, velocity, and pressure. In view of the incompressible and steady flow, the Reynolds-averaged Navier–Stokes governing equations can be written as [26, 30].

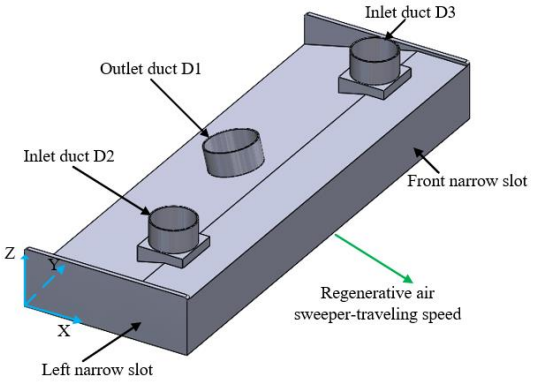


Fig.3 Physical model regenerative air sweeper pick-up head Mathematical model Flow field equations

Continuity: $\frac{\partial u_i}{\partial x_i} = 0$ (1)

Where u_i is the airflow velocity.

Momentum: $\frac{\partial}{\partial x_j}(\rho u_i u_j) = -\frac{\partial P}{\partial x_i} + \frac{\partial}{\partial x_j}\left(\mu \frac{\partial u_i}{\partial x_j} + T_{ij}\right) + \rho g_i$ (2)

Where ρ, P, and μ are the fluid density, pressure and viscosity, respectively. $g_i$is the gravity acceleration. $T_{ij} = -\rho u_i' u_j'$ is the Reynolds stress

The selection of turbulence models for the prediction of flow field characteristics is dependent on the physical model used. The k–ε model is widely used for dust-collection and sweeper vehicles, k is the turbulent kinetic energy; ε is the kinetic energy dissipation coefficient and it can provide accurate predictions for complex flows. The k–ε equation is written as follows:

$$\rho \frac{dk}{dt} = \frac{\partial}{\partial_{xj}}\left[\left(\mu + \frac{\varepsilon_m}{\sigma_k}\right)\frac{\partial k}{\partial xj}\right] + G_k - \rho\varepsilon \quad (3)$$

$$\rho \frac{d\varepsilon}{dt} = \frac{\partial}{\partial_{xj}}\left[\left(\mu + \frac{\varepsilon_m}{\sigma_\varepsilon}\right)\frac{\partial k}{\partial xj}\right] + C_{1\varepsilon}\frac{\varepsilon}{k}G_k - C_{2\varepsilon}\rho\frac{\varepsilon^2}{k} \quad (4)$$

Where $G_k = -\rho u_i' u_j' \frac{\partial u_i}{\partial_{xj}}$, and the constants are listed in the following table 1.

Table 2. k–ε model

σ_k	$C_{1\varepsilon}$	$C_{2\varepsilon}$	σ_ε
1.0	*1.44*	*1.92*	*1.3*

Particle movement within the system

The Euler–Lagrange approach was used to predict the particles' trajectories within the regenerative vacuum cleaning system. The airflow and particles were treated as continuous and disposed phases, respectively. The continuous phases were described with Navier–Stokes governing equations. A discrete-phase model (DPM) was used to describe the physical properties of the particles because the volume fraction was less than 10%[26].

The force balance equation based on Newton's Second Law can be written as [26]

$$m_p \frac{dU_p}{dt} = F_d + F_g + F_s \quad (5)$$

Where m_p is the particle mass, U_p *is* the particle velocity, F_D is the drag force, F_g is the gravitational force, F_s is the particle lifting force.

The drag force F_D can be written in terms of the drag coefficient C_D as follows [10, 31]

$$F_D = \frac{18\mu}{\rho_\rho d_\rho^2}\frac{C_D R_e}{24} m_\rho (U - U_\rho) \quad (6)$$

Where ρ_ρ is the particle density, d_ρ is the particle diameter, and R_e is the relative Reynold number, considering the particle shape, the drag coefficient C_D is defined by the correlations developed by Haider [32].

The gravitational force F_g can be written as [5, 26]

$$F_g = m_\rho(1 - \rho/\rho_g)g \quad (7)$$

The drag coefficient can be obtained from [18, 19, 32]

$$C_D = (2.25Re^{-0.31} + 0.36Re^{0.06})^{3.45} \quad (8)$$

Free suspension velocity of spherical object can be known. The suspension velocities of spheres in different fluid regions are different. This area is the pressure differential resistance zone because of the inhalation of the larger size particles.

Particle lifting force F_s can be written us [5, 26]

$$F_s = \frac{2K_v^{0.5}\rho d_{ij}}{\rho_p d_p (d_{lk}d_{kl})^{0.25}}(U - U_p) \quad (9)$$

Where ρ_p and d_p are the density and diameter of the particle, U is the air velocity, v is the kinematic velocity, k is the turbulence kinetic energy, d_{ij} is the deformation tensor, and the constant is K=2.594 [33, 34]

The Reynolds number for a spherical particle is given by[23, 35]

$$R_e = \rho(u - u_p)d_p/\mu \quad (10)$$

Starting velocity analysis of dust particles

The dust particle is the primary working object of the fan suction system. The starting velocity of dust particles is the least gas flow velocity required by dust particles from static to moving state. When the flow velocity exceeds the minimum starting speed of dust particles can the dust particles change from quiescence to motion. The starting velocity of the dust particles in a horizontal circular pipe has been obtained.

For a single dust particle:[7, 13, 22]

$$U_s = \left[1 - \left(\frac{d_p}{D}\right)^{1.5}\right]\sqrt{\frac{4fgd}{3C_D}\left(\frac{\rho_p - \rho}{\rho}\right)}, \quad (11)$$

For a small single sphere, the following equation was found[16]:

$$1.54 \cdot 10^{-4}\left[1 - \left(\frac{d}{D}\right)^{1.5}\right]^{-2} C_D \rho d^4 \left(\frac{U_s^7}{\nu^3 D}\right)^{\frac{1}{2}} = f\left[\frac{\pi}{6} g d^3(\rho_c - \rho) + 1.302 \cdot 10^{-6} d - 6.35 \cdot 10^{-3}\rho d^3 \left(\frac{U_s^{21}}{\nu^5 D^3}\right)^{1/8}\right] \quad (12)$$

For the stratified accumulation of the particles:

$$U_p = \left(1.27Ar^{-1/3} + 0.36Ar^{-1/4} + 0.45\right) * \left(0.70Ar^{-1/5} + 1\right)U_s \quad (13)$$

For the Archimedes number:

$$Ar = \frac{g\rho(\rho_c - \rho)d^3}{\mu^2} \quad (14)$$

Where $U_s$is the starting velocity of a single dust particle, m/s; d is the dust particle diameter; $U_p$is the incipient velocity of stratified dust particles; D is the diameter duct; $C_D$is the drag coefficient; $\rho_p$is the true density of dust particles; ρ is the air density; f is the friction coefficient between dust particles and duct, Ar is the Archimedes number, and μ is dynamic viscosity coefficient of air, 1.84-5$Pa \cdot s$. Through the calculation of 13 equations, the suction mouth needs suction wind speed of 30m/s providing by the port at least, so all of them are pick- up.

They assumed that the pickup velocity is defined by the vertical lift-off (vertical force balance) and have found that[13, 15, 36]:

$$U_{pu} = \frac{2.62\nu^{13/21}D^{3/21}}{\mu^{8/21}}\left[\frac{\pi}{6}g\left(\rho_p - \rho\right) + \frac{1.302 \cdot 10^{-6}}{d^2}\right]^{8/21} \quad (15)$$

where D is the duct diameter and ρ_p is the particle density.

Boundary conditions and Solution Controls

The discrete phase model (DPM) was referred to the physical properties of particles and to determine the trajectory of particle motion. The rosin-Rammler model is used for the particle size distribution. The particle physics model is chosen to be spherical, during the simulation, a discrete random walk model was adopted in[5, 26]. Initialize compute from all zones. Dust and particle-wall interactions are modeled by reconstruction coefficients that determine the amount of momentum in the normal (or tangential) direction on a wall held by a particle after it collides with a wall. In this simulation, it was assumed that the collisions between particles of different types and walls were not elastic. The efficiency of particle removal was tested by removing a certain number of particles from the injection surface and observing the number of particles emitted through the outlet of the pickup head. The main features of the simulation are presented in table 4. In general, the overall removal efficiency of the dust and particles was taken to evaluate the particle removal efficiency of the road sweeper pick-up head.

Total removal efficiency is the proportion of the number of particles removed from the road surface to the total number of particles to inculcate per reception, regardless of the type and composition of the waste. Overall removal efficiency, and can be defined by:

$$\eta = \frac{G_1}{G_2} \cdot 100\% \quad (16)$$

Where η is the overall removal efficiency; G_1 is the inlet mass flow rate, kg/s; G_2 is the removal mass flow rate (also called the outlet mass flow rate), kg/s.

It is generally necessary to determine the weight of the particles first in order to determine the efficiency of the collection of particles on the road surface during the experiment. A reliable way to determine the efficiency of particles on the road surface is to ascertain the efficiency depending on the change in the mass of the particles. The additional efficiency is a method that describes how well the particles are removed from the road surface depending on the particle size and mass distribution. The ratio of the number and mass of particles on the road surface of the particles collected to determine the suction efficiency of the particles for the experimental results. By analogy with Eq. (16), the road surface particle collection efficiency η_w is defined as

$$\eta_w = \frac{P_m}{P_m + P_{pm}} \cdot 100\% \qquad (17)$$

Where η_w is the efficiency of road surface particle collection, η_m is the mass of the total particles on the road surface, η_{rm} is the mass of residual particles after collection on the road surface, kg.

The density of particles usually located on the road surface has a high effect on the absorption efficiency, Table 3 describes the particle density.

Table 3. The density of a large particle on the road surface

Material	*Wood*	*Sand*	*Clay (wet)*	*Asphalt*	*Glass*
Density(kg/m^3)	*600*	*1650*	*2080*	*2400*	*2500*

Table 4.

Feature	***Gas phase***	***Feature***	***Solid phase***
Fluid	*Air*	*Particle diameter distribution*	*Rosin- Rammler*
Compressibility	*Incompressible*	*Mass velocity (kg/s)*	*0.5*
Dimensions	*3D*	*Gaz density, (kg/m^3)*	*1.225*
Time dependence	*Steady state*	*Spread parameter, n*	*5.95*
Turbulence model	*k-epsilon (2eqn)*	*Min particle diameter (μm)*	*50*
Inlet condition	*Velocity inlet*	*Max particle diameter (μm)*	*250*
Outlet condition	*Pressure outlet*	*Particle mean diameter (μm)*	*125*

Result and discussion

Initial flow rate of particle removal efficiency

The effect of particle shape on suction mouth pick-up velocity is briefly mentioned, but it is possible to determine the velocity of particles in real state by conducting experiments on a regenerative air sweeper test-rig to determine a specific relationship with the pick-up velocity. By studying the effect of particle shape, the sweeper suction efficiency indicates the presence of a minimum collection rate. In most cases, the waste particles on the road surface are in discrete dimers, in road sweepers it is usually very difficult to clean small heavy particles [13, 14]. Fig. 5 Illustration the calculation and experimental results of the dust starting velocity. The used in equation (5) to calculate the starting velocity of the particles. The period of motion of the particles on the surface of the conveyor belt was taken into account in the experimental determination. When waste and particle density of 600 kg/m^3 and a particle size of 3 mm to 30 mm are assumed. There experimental results were higher

than the calculated results. The particle size is on average 22% of the difference in the starting velocity of particles in the range of 3mm, the closest difference in the velocity of motion of the particles was in the 24 mm to 27 mm-sized particles. This difference was 4%.

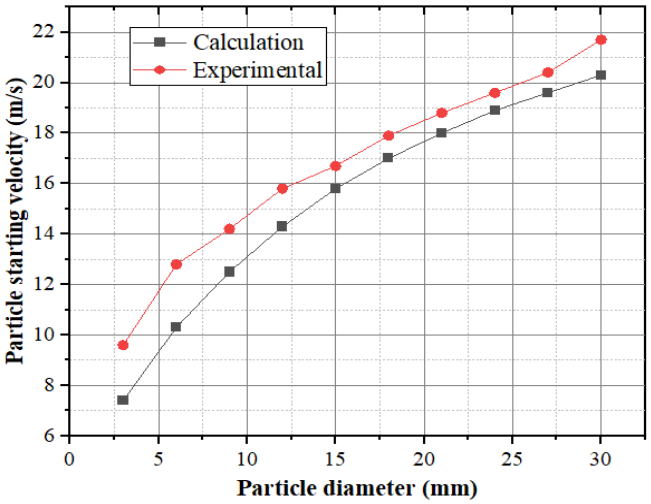


Fig-5. The calculation and experimental results of the particle starting velocity

Particle suction removal efficiency

The experiment was conducted in the laboratory of the Suzhou Inspection Center at Wuhan University of Technology. A special conveyor belt acts as a sweeper movement speed and road surface. Sand particles in sizes from 63μm to 200μm are used. it is possible to determine the sweeper removal effect of particles of this size by experiment as well as by simulation method. The conveyor uses dust feeder to control the movement of the particles to ensure that the particles on the belt surface are evenly distributed. The mass-calculation method was used is efficiency of dust and particle intake was determined by calculating the mass of granite particles before and after dust collection [5, 11, 26, 37]. Figure 6 shows the analysis of different speed of sweeper movement and the results of the overall dust removal efficiency test. By comparing the CFD numerical calculation with the experimental data, we observe how the simulation results differ from the experimental[8, 23]. The simulation data were higher than the experimental results when measured. The simulation and test results were very close to each other when traveling-speed ranges from 6 km/h to 10 km/h. There difference in results between the traveling-speed 12 km/h and 18 km/h significantly increased. The difference between the results at a traveling-speed of 18km/h was 15%.

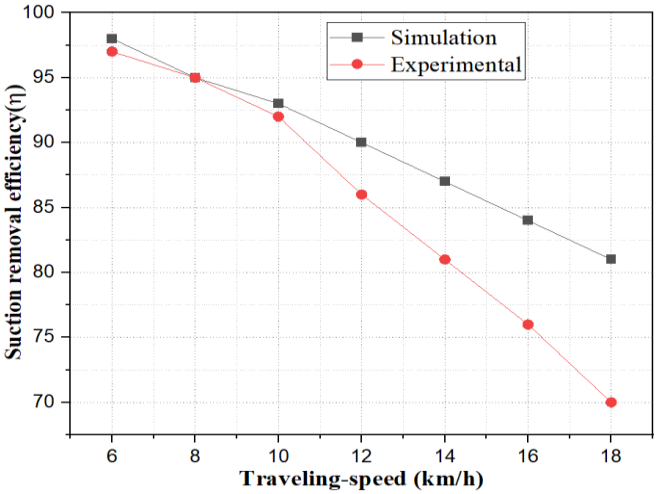


Fig. 6. Comparison of suction removal efficiency between experiment and simulation

Effect of pressure change on particle removal efficiency

Fig. 7 shows the effects of the pressure drop on particle removal efficiency. The small-scale efficiency decreases slightly with decreasing pressure, but for large-sized particles it increases significantly. A drop in pressure has a clear effect on efficiency at levels ranging from 1800 Pa to 2100 Pa, for large-sized particles, the efficiency of wig removal for a pressure drop from 2100 Pa to 2400 Pa does not increase significantly, but a relatively high efficiency is achieved at 2400 Pa. Experience has shown that it is possible to control relatively small particles, and to pressure 2400 Pa the removal effect is higher than 0.96 η when the particle size is 10 mm.

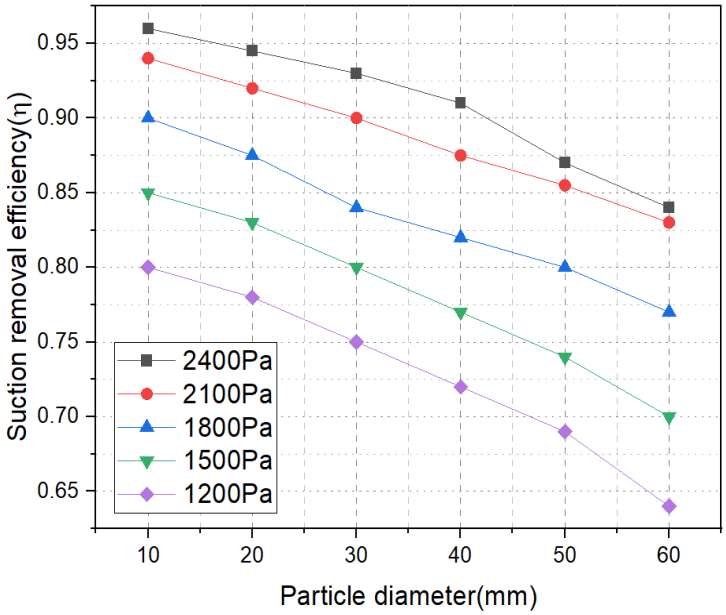


Fig. 7. Effects of pressure drop on suction removal efficiency

Conclusion

This study involves measuring and evaluating factors affecting particle removal efficiency in an improved pick-up head model of a regenerative air vacuum sweeper. The results of numerical simulation were confirmed by conducting experiments using a specially developed experimental setup system.

The simulation results show that the structure and mass of the particles, sweeper speed, the distance between the pick-up head and the road surface clearly affects the efficiency of particle removal. In many cases, the composition of waste and particles on the road surface will vary. Simulation and experiments have shown that the change in particle weight relative to the change in particle size has a higher effect on cleaning efficiency. If the velocity and pressure of the airflow in the suction mouth of the particles of the pick-up head are insufficient, which leads to a decrease in efficiency and affects the lifting and removal of road surface particles.

High sweeper speed leads to a shortening of the sweeping period by removing particles from the road surface. The regenerative air sweeper has a superior suction removal efficiency during changes in particle composition and different road conditions when moving at a speed of 5 km/h to 10 km/h.

Reference

1. Bao, Y. and Z. Zhang. Development and performance analysis of a small road sweeper and dust collector. in 2021 3rd International Symposium on Robotics & Intelligent Manufacturing Technology (ISRIMT). 2021. IEEE.

2. Avsar, E., et al., Investigation of PM10 Concentrations and Noise Levels of the Road Sweepers Operating in Istanbul-Turkey: A Case Study. Fresen. Environ. Bull, 2010. 9(19): p. 2033-2039.
3. Chang, Y.-M., et al., Effectiveness of street sweeping and washing for controlling ambient TSP. Atmospheric Environment, 2005. 39(10): p. 1891-1902.
4. Calvillo, S.J., E.S. Williams, and B.W. Brooks, Street dust: implications for stormwater and air quality, and environmental management through street sweeping. Reviews of Environmental Contamination Toxicology Volume 233, 2015: p. 71-128.
5. Wu, B., J. Men, and J. Chen, Numerical study on particle removal performance of pickup head for a street vacuum sweeper. Powder technology, 2010. 200(1-2): p. 16-24.
6. Wu, B., J. Men, and J. Chen, Study of the Particle Separation Performance of a Dust-settling Hopper. Chemical Product and Process Modeling, 2011. 6(1).
7. Zhang, H.-j., X.-f. Wang, and K.-k. Liu, Simulation and Optimization of Fan System for Road Sweeper. Journal of Highway Transportation Research Development, 2018. 12(4): p. 92-97.
8. Cai, S., et al., Parameters optimization of the dust absorbing structure for photovoltaic panel cleaning robot based on orthogonal experiment method. Journal of cleaner production, 2019. 217: p. 724-731.
9. Chen, X., et al. Numerical Analysis of a Centrifugal Fan for a Road Sweeper. 2017.
10. Xi, Y., et al. Numerical study on particle suction performance of reverse blowing pickup mouth. in Journal of Physics: Conference Series. 2018. IOP Publishing.
11. Xi, Y., et al., Enhancement of particle collection efficiency considering the structural interplay: particle motion characteristics analysis. Mechanics Industry, 2020. 21.
12. Daichin and S. Lee, Experimental analysis of flow fields inside intake heads of a vacuum cleaner. Journal of Mechanical Science Technology, 2005. 19: p. 894-904.
13. Kalman, H., et al., Pickup (critical) velocity of particles. Powder technology, 2005. 160(2): p. 103-113.
14. He, Y., et al., Ga• Solid Turbulent Flow in a Circulating Fluidized Bed Riser: Experimental and Numerical Study of Monodisperse Particle Systems. Industrial Engineering Chemistry Research, 2009. 48: p. 8091-8097.
15. Hayden, K.S., K. Park, and J.S. Curtis, Effect of particle characteristics on particle pickup velocity. Powder Technology, 2003. 131(1): p. 7-14.
16. Cabrejos, F.J. and G. Klinzing, Incipient motion of solid particles in horizontal pneumatic conveying. Powder Technology, 1992. 72(1): p. 51-61.
17. Cabrejos, F.J. and G.E. Klinzing, Pickup and saltation mechanisms of solid particles in horizontal pneumatic transport. Powder Technology, 1994. 79(2): p. 173-186.
18. Neilson, J.H. and A. Gilchrist, An analytical and experimental investigation of the velocities of particles entrained by the gas flow in nozzles. Journal of Fluid Mechanics, 1968. 33(1): p. 131-149.
19. Neilson, J.H. and A. Gilchrist, An analytical and experimental investigation of the trajectories of particles entrained by the gas flow in nozzles. Journal of Fluid Mechanics, 1969. 35(3): p. 549-559.
20. Li, A. and G. Ahmadi, Dispersion and deposition of spherical particles from point sources in a turbulent channel flow. Aerosol science technology, 1992. 16(4): p. 209-226.
21. Park, I.-S., et al., Flow-induced noise in a suction nozzle with a centrifugal fan of a vacuum cleaner and its reduction. Applied Acoustics, 2010. 71: p. 460-469.
22. JiaQiang, E., et al., Simulation on Entrainment Process of Suction Mouth under Negative Pressure in the Medium Dry Sanitation Trucks. Applied Mechanics Materials, 2014. 711: p. 86 - 90.

23. Wu, B., J. Men, and J. Chen, Improving the design of a pickup head for particle removal using computational fluid dynamics. Proceedings of the Institution of Mechanical Engineers, Part C: Journal of Mechanical Engineering Science, 2011. 225(4): p. 939-948.

24. Zhaowen, J., C. Kai, and G. Yuming, Nozzle system performance analysis for suction broom road sweeper [J]. Special Purpose Vehicle, 2012. 6: p. 92-97.

25. Gilbert, M., L. Davis, and D. Altman, Velocity lag of particles in linearly accelerated combustion gases. Journal of Jet Propulsion, 1955. 25(1): p. 26-30.

26. Xi, Y., et al., Prediction of particle-collection efficiency for vacuum-blowing cleaning system based on operational conditions. Processes, 2020. 8(7): p. 809.

27. Zeng, G.-y., et al., Simulation for the design of dust suction system of highway sweeper. Syst. Simul, 2004. 16(12): p. 2770-2773.

28. Jiaqiang, E., et al., Simulation on entrainment process of suction mouth under negative pressure in the medium dry sanitation trucks. Applied Mechanics Materials, 2015. 711: p. 86-90.

29. Jiaqiang, E., et al. Simulation optimization on sucking up dust particle by suction mouth in sanitation sweepers under the negative pressure. in 2015 International Forum on Energy, Environment Science and Materials. 2015. Atlantis Press.

30. Xin, Y.H., H. Li, and J.J. Wu. Applications of CFD Technique in the Flow Field Analysis of Road Sweeper. in Applied Mechanics and Materials. 2015. Trans Tech Publ.

31. Tan, G., et al., Vacuum Cleaning Vehicle Dust Subsidence System Design. 2014, SAE Technical Paper.

32. Haider, A. and O. Levenspiel, Drag coefficient and terminal velocity of spherical and nonspherical particles. Powder technology, 1989. 58(1): p. 63-70.

33. Saffman, P.J., The lift on a small sphere in a slow shear flow. Journal of Fluid Mechanics, 1965. 22: p. 385-400.

34. Koshkarev, S.A., A.I. Evtushenko, and P.A. Roschin. Modeling of cleaning of dust emission in fluidized bed building aspiratioŽ collector. 2017.

35. Shen, H., et al., Influence of Gas Flow Speed on Laser Plume Attenuation and Powder Bed Particle Pickup in Laser Powder Bed Fusion. JOM, 2020. 72: p. 1039-1051.

36. Zhou, J., L. Xu, and C. Du, Prediction of lump coal particle pickup velocity in pneumatic conveying. Powder Technology, 2019. 343: p. 599-606.

37. Aliukov, S. and K. Osintsev, Mathematical modeling of coal dust screening by means of sieve analysis and coal dust combustion based on new methods of piece-linear function approximation. Applied Sciences, 2021. 11(4): p. 1609.

TOSHKENT DAVLAT TRANSPORT UNIVERSITETI
Tashkent state transport university
International Journal Of Transport And Technological Machines
Tashkent 2024, issue 1, https://ijttm.uz/

REDUCING THE DANGER OF PASSING CONFLICTS IN TRAFFIC FLOW AT CONTROLLED INTERSECTIONS USING VEHICLE DETECTORS

D. V. Kapsky[1)], A.A.Mukhitdinov[2)]
[1)] *Doctor of Technical Sciences, Professor of the Belarusian National Technical University, Minsk, Republic of Belarus*
[2)] *Doctor of Technical Sciences, Professor of the Tashkent State Transport University, Tashkent, Republic of Uzbekistan*
[1)] *email: d.kapsky@gmail.com*
[2)] *Corresponding author: akmalmukhitdinov@gmail.com*

Abstract. The article presents the results of experimental and analytical studies to identify dilemma areas, taking into account the specifics and conditions of traffic at signalized intersections. This dilemma zone is formed due to the fact that the driver is faced with the problem of making a decision when transferring the right to move from one (traffic) stream to another: to slow down and stop the car before the intersection or to continue driving and enter the intersection. As a rule, the decision to continue driving is accompanied by an increase in speed in order to leave (vacate) the intersection before the red light turns on in accordance with the requirements of the Traffic Rules. This circumstance increases the potential danger of interphase conflicts that arise at the intersection when transferring priority.

Depending on the distance to the intersection and the speed of traffic, drivers may not be confident that they will stop in time, or they may be confident that they will leave the intersection before the conflicting traffic begins to move, which creates an area of dilemma and in turn leads to accidents (mainly collisions with a blow from behind). It was found that with constant duration of green flashing and yellow signals, the dilemma area increases with increasing speed; for constant speed and constant duration of green flashing and yellow signals, increasing deceleration or acceleration leads to a decrease in the dilemma area; increasing the size of the intersection directly increases the length of the dilemma zone.

It has also been established that multipoint detector systems are more acceptable for traffic light objects where high speeds or a large spread of speeds occur, as well as the fact that an excessive increase in transition intervals does not always lead to a positive result, especially since this leads to an increase in delays and stops Vehicle.

Key words: accident reduction, signalized intersection, vehicle detectors, dilemma zone, interphase conflicts, conflicting flow, multipoint detector systems.

Introduction

There is a problem that worries designers, safety and traffic management specialists [1], [2]. Drivers approaching an intersection are often faced with the dilemma of whether to stop or continue through the intersection when the green light is flashing or when the yellow light begins to glow.

Research has been conducted on detector placement to reduce this problem [3], [4]. The article identifies a number of factors that influence the problem of the “dilemma zone” and describes several detector layouts that have proven to be effective in accordance with the control algorithms used at these sites [5]–[8].

Analysis of vehicle traffic conditions when transfering the right to drive

If the driver decides to stop, then after a short decision time he begins to brake [9], [10]. The distance the vehicle travels after the green light starts flashing includes the distance traveled during the decision time and the distance traveled during the braking time. The following inequality should guarantee a safe stop [8], 11]

$$X \geq v \cdot t + \frac{v^2}{2d}, \qquad (1)$$

here: X – distance to the stop line when the green flashing light turns on, м;
v – the speed at which the car is moving, m/s;
t – decision making time (usually 1 s);

d – car deceleration, m/s^2.

Safe and comfortable braking occurs if the vehicle deceleration does not exceed one third of the free fall acceleration. Using d* to denote the critical deceleration under normal road conditions, then the braking distance can be defined as

$$X_S = v \cdot t + \frac{v^2}{2d*}. \quad (2)$$

The Xs value is the minimum distance to the stop line at which the car can stop safely and comfortably after the green signal starts flashing. The area between the stop line and the Xs zone is a zone in which drivers are not expected to stop, “no stopping” (Fig. 1).

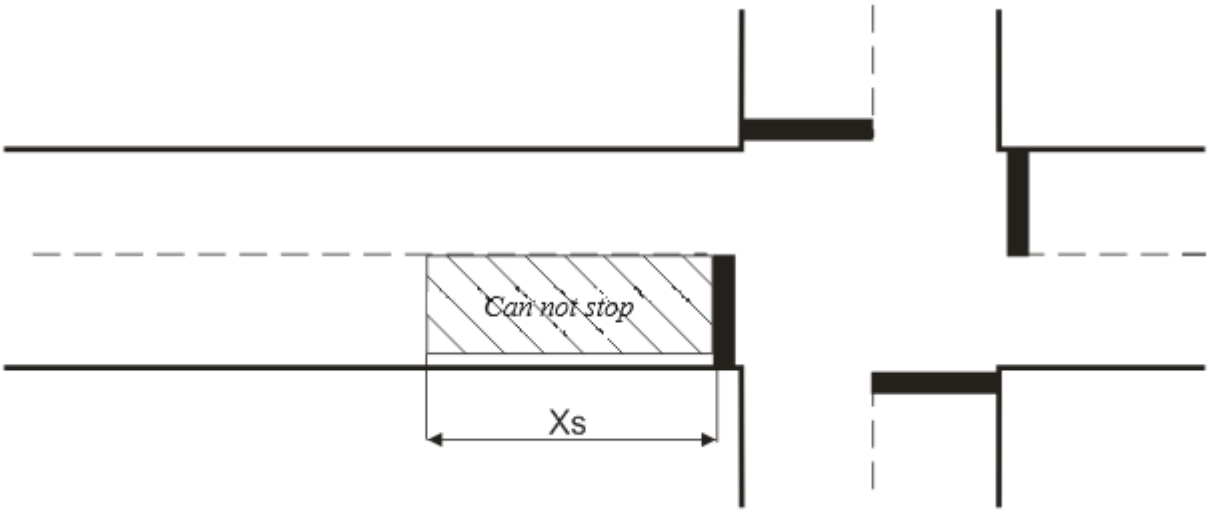


Figure 1. “Can’t stop” zone

If the driver decides to increase his speed and drive through the intersection, then the following inequality must hold:

$$Xc \le v(Gf + Y) + \frac{a(Gf + Y - t)^2}{2} - (W + L), \quad (3)$$

где Xc – safe distance, m;
Gf – green signal blinking time, s;
Y – time of yellow traffic light, s;
a – vehicle acceleration, m/s ^{2};
W – intersection width, m;
L – intersection width, m.

The resulting inequality allows the driver to leave the intersection before the red light turns on.

The acceleration acceptable to the driver can be obtained from the expression

$$a = 4{,}9 - 0{,}213v, \quad (4)$$

From this expression it can be seen that greater acceleration can be achieved if the driver drives at a lower speed [12], [13]. Distance Xc is the maximum distance from the stop line from which the driver can drive through the intersection before the red light turns on. Xc can be defined as:

$$Xc = v(Gf + Y) + \frac{a(Gf + Y - t)^2}{2} - (W + L). \quad (5)$$

It is expected that all cars located further than the distance Xc will not be able to pass the intersection before the red light starts flashing and thus they will be in the “no moving” zone (Fig. 2).

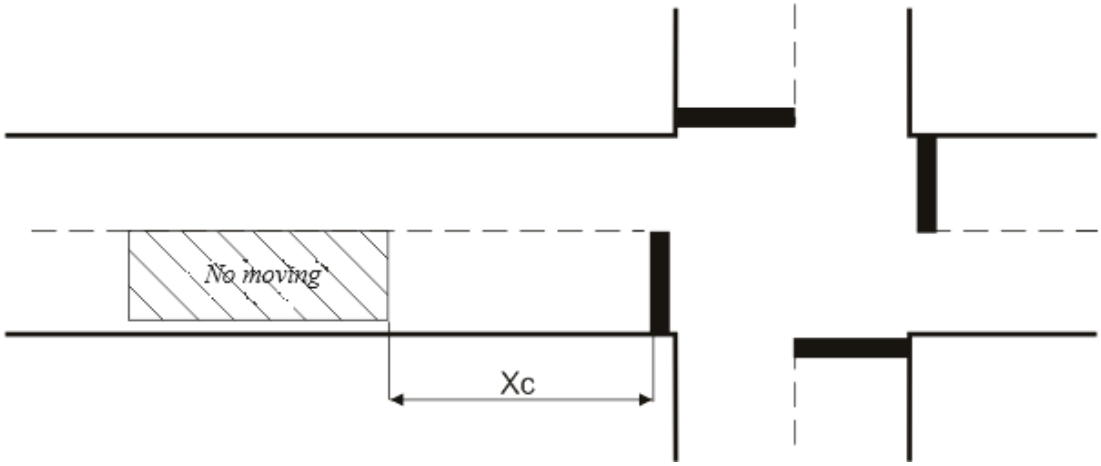


Figure 2. “No moving” zone

Since Xs and Xc are easily calculated distances, their relationship can be expressed by one of the following inequalities:

$$Xs > Xc,$$
$$Xs = Xc,$$
$$Xs < Xc.$$

In the first case, when Xs > Xc, an overlap zone appears in which the driver can either stop or continue driving when the green signal flashes. This zone is called the “dilemma zone” (Fig. 3). In this case, the driver of one vehicle in the dilemma area may brake at the start of the green light flashing, while the driver of the other vehicle may accelerate, resulting in an increased risk of side or rear-end collisions [6], [8], [13], [14].

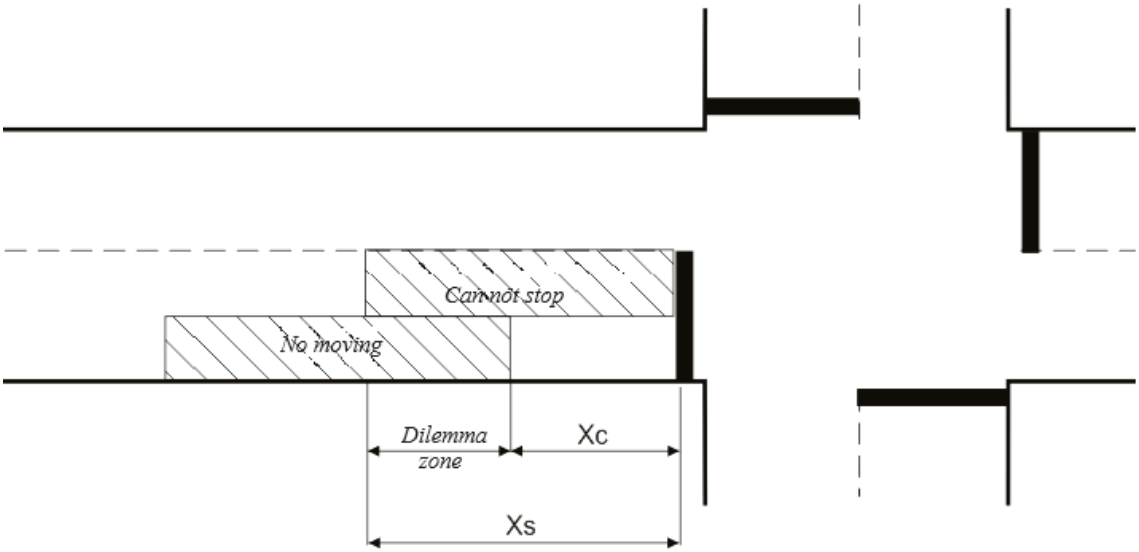


Figure 3. Dilemma zone (*Xs > Xc*)

In the case when Xs = Xc, the dilemma zone disappears and therefore the problems described in the previous paragraph do not exist (Fig. 4). Drivers in a "No Moving" zone will be able to stop safely and calmly, while drivers in a "No Stopping" zone will be able to successfully accelerate through the intersection.

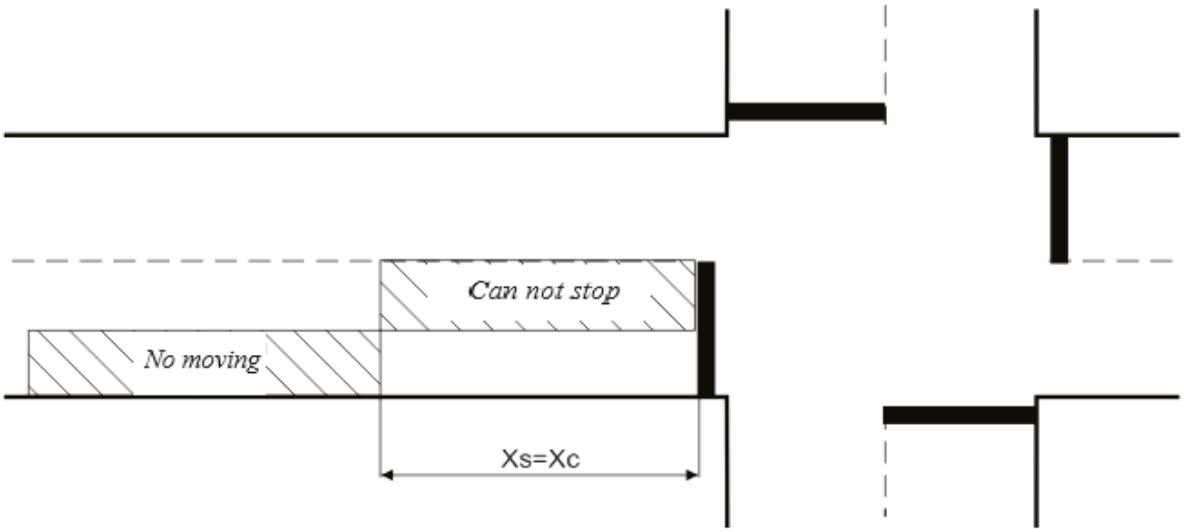


Figure 4. No dilemma zone (*Xs = Xc*)

In the third case, when Xs < Xc, in the zone between Xs and Xc the driver can both stop and brake safely. Therefore, this zone is considered as a free choice zone (Fig. 5).

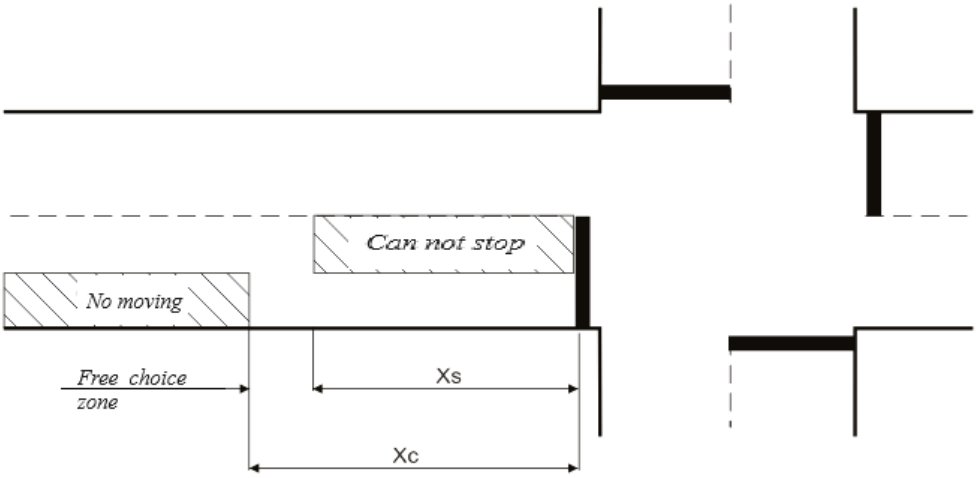


Figure 5. Free choice zone (*Xs < Xc*)

From this simple analysis it can be seen that a dilemma zone appears if Xs > Xc. From expression (2) and (5) it can be seen that Xs is a function of speed, decision time and deceleration, while Xc is a function of speed, decision time, acceleration, green flashing time, yellow flashing time and intersection dimensions. By analyzing and comparing these functions, several main conclusions can be drawn:

- with a constant duration of green flashing and yellow signals, the dilemma area increases with increasing speed;

- for constant speed and constant duration of green flashing and yellow signals, an increase in deceleration or acceleration leads to a decrease in the dilemma area;

- increasing the size of the intersection directly increases the length of the dilemma zone.

In a strict control mode of a traffic light object, the problem of the “dilemma zone” is usually solved by increasing the transition interval, which in turn leads to an increase in vehicle delays.

In adaptive traffic light control, the problem of "dilemma zone" can be solved by properly positioning vehicle detectors [12], [14]. In this case, detectors can be placed before, within, or after the dilemma zone to reduce the likelihood of a vehicle entering the dilemma zone when the green light begins to flash.

Depending on the control algorithms, we will consider three main ways of arranging detectors.

Control algorithms that increase the duration of the green signal

In this case, the peripheral technical means of traffic management include two inductive loops (detectors). The concept of this control algorithm is very simple and consists of finding the car before it gets into the dilemma zone, and then increasing the duration of the green light until the car leaves the dilemma zone.

The layout of the detectors is shown in Figure 6. The location of the frames in this case is determined by the 85% confidence interval of the velocities. The following expressions are used to find the distance to the frames:

$$D = 0,44v\,t_1 + \frac{0,003v^2}{\varphi}, \quad D = v \cdot t_1 + \frac{v^2}{20\varphi}, \tag{6}$$

$$D_2 = 1,47v\left(\frac{v}{30} + 1\right), \tag{7}$$

$$D_1 = D - D_2, \tag{8}$$

here v – 85% confidence interval of speed, m/s;
t_1 – driver reaction time, s;
φ – adhesion coefficient;
D – stopping distance, m;
D_1 – stopping distance, m
D_2 – interval between frames, m.

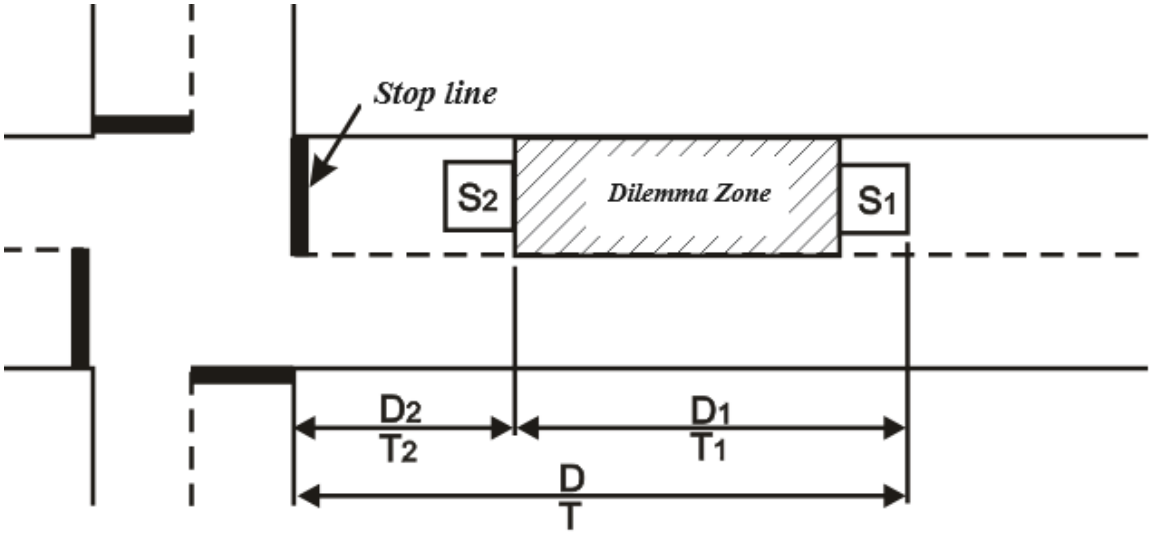


Figure 6. Using two detectors for the algorithm for increasing the duration of the green signal

Assuming the frames are positioned as shown above, a car passing over frame S1 will activate a timer which will increase the duration of the green signal in order for the car to reach frame S2 in time T1. At the same time, when the car passes over frame S2, the second timer will keep the green signal until the car reaches the intersection. This scheme does not

guarantee that if a car is traveling at a speed that falls within the 85% confidence interval, then it will not enter the dilemma zone.

Calling algorithm

This concept uses a 21 m presence frame located upstream of the stop line and a small call detector located 75–150 m from the stop line (Fig. 7). The value of D is calculated using formula (6), and the 85% confidence interval of the speed or the maximum permitted speed is also used. D2 is equal to 21 meters. T1 is set adequately by D1 (which is equal to D – D2) divided by the lower rate, which basically corresponds to the 15% confidence interval. This time is set on the call detector timer. The road controller operates in presence control mode.

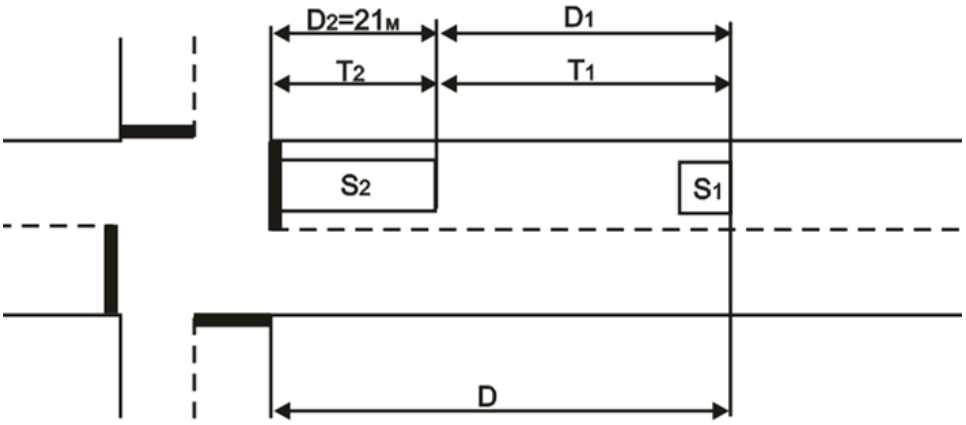


Figure 7. Using a calling detector

This scheme ensures that the last car before a gap in traffic and cars traveling below the speed limit do not get caught in the dilemma. Trailing vehicles may end up on the end of the extended green signal. The 21-meter presence frame ensures that vehicles stopped while the light is red will leave the intersection without the gap being detected prematurely.

Multipoint detector algorithms

The two methods described above use two detectors each. These methods can be used effectively at low speed intersections. As discussed above, as speed increases, the dilemma area increases, and therefore more detectors are needed to accommodate a wide range of driving speeds. In world practice, there are a number of methods for determining the location of detectors. Let's consider one of them.

The technique uses one-second intervals of vehicle movement. The furthest detector from the intersection is located at the safe stopping distance from the intersection for the highest speed (Figure 8). The safe stopping distance is based on a reaction time of 1 second plus braking distance, corresponding to a friction coefficient of 0.41–0.54 for speeds of 30–90 km/h. The next detector is located at a safe stopping distance for vehicles traveling at a speed 15 km/h less than that set for the first detector. If the travel time between two detectors is more than 1 s, then the second detector is moved so that cars can reach it within 1 s set in the controller.

This procedure for installing the frame is repeated until the last frame is located at a distance of about 23 m from the stop line, each time reducing the speed by 15 km/h relative to the one in question. The minimum duration of the green signal is set in the controller so that vehicles stopped between the last detector and the intersection can leave it.

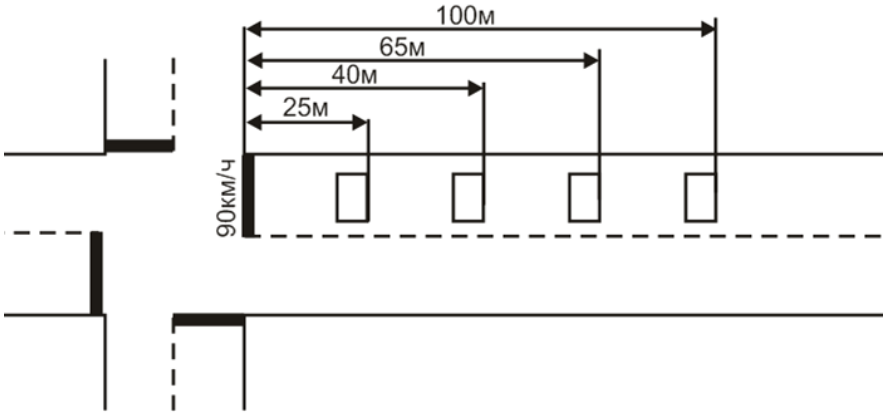


Figure 8. Installation of multipoint detectors

Since the length of the dilemma zone increases with increasing speed, more detectors are needed to guide cars through the dilemma zone. In addition, the greater the interval between detectors, the greater the interval between vehicles and the less efficient the controller.

As practice has shown, multipoint detector systems are more suitable for objects where there are high speeds or there is a large spread of speeds.

Conclusion

The existence of the dilemma zone problem should first of all be paid attention to by specialists responsible for the design of traffic light facilities, as well as road safety specialists. Side-impact and rear-end vehicle collisions remain the primary collisions at these sites. An excessive increase in transition intervals does not always lead to a positive result, especially since it leads to increased delays and vehicle stops. The correct use of vehicle detectors will allow them to be used as an additional tool in solving this problem.

Reference

1. Road safety: development paradigms: a manual for preparing masters when studying module T1-E1 “Basic concept of road safety” / D. V. Kapsky [et al.]. – Minsk: Capital Print, 2017. – 264 p.

2. Komarov, V.V. Architecture and standardization of telematic and intelligent transport systems. Foreign experience and domestic practice / V. V. Komarov, S. A. Garagan. – M.: NTB “Energia”, 2012. – 352 p.

3. Evstigneev, I. A. Fundamentals of creating intelligent transport systems on federal roads of Russia / I. A. Evstigneev. – M.: Pero, 2016. – 260 p.

4. Dushkin, R.V. Intelligent transport systems / R.V. Dushkin. – M.: DMK Press, 2020. – 282 p.

5. Intelligent transport systems. Architecture of intelligent transport systems. Technical requirements. Service domains of intelligent transport systems, service groups and services: STB 2556-2019 (ISO 14813-1:2015).

6. Kapsky, D.V. Methodology for improving the quality of road traffic: monograph / D.V. Kapsky. – Minsk: BNTU, 2018. – 372 p.

7. Modern trends in the development of on-board intelligent transport systems: monograph / D. V. Kapsky [et al.]. / SPbGASU. – St. Petersburg, 2019. – 298 p.

9. Kapsky, D. V. Method for predicting road traffic accidents based on potential danger / D. V. Kapsky - M.: New knowledge, 2015. - 327 p.

10. Abdurazzokov, U., Sattivaldiev, B., Khikmatov, R., & Ziyaeva, S. (2021a). Method for assessing the energy efficiency of a vehicle taking into account the load under operating conditions. E3S Web of Conferences, 264, 05033. https://doi.org/10.1051/e3sconf/202126405033

11. Abdurazzokov, U., Sattivaldiev, B., Khikmatov, R., & Ziyaeva, S. (2021b). Method for assessing the energy efficiency of a vehicle taking into account the load under operating conditions. E3S Web of Conferences, 264, 05033. https://doi.org/10.1051/e3sconf/202126405033

12. Dashdamirov, F., Abdurrazzokov, U., Ziyaev, K., Verdiyev, T., & Javad-li, U. (2023). Simulation testing of traffic flow delays in bus stop zone. E3S Web of Conferences, 401, 01070. https://doi.org/10.1051/e3sconf/202340101070

13. Faizullaev, E. Z., Rakhmonov, A. S., Mukhtorjanov, U. M., Turdibekov, S., & Nasirjanov, Sh. I. (2023). Parameters of the access road for disaster situations on the roads in the mountain area. E3S Web of Conferences, 401, 03022. https://doi.org/10.1051/e3sconf/202340103022

14. Fayzullaev, E., Tursunbaev, B., Xakimov, S., & Rakhmonov, A. (2022). Problems of vehicle safety in mountainous areas and their scientific analy-sis. 030099. https://doi.org/10.1063/5.0089596

15. Fayzullayev, E., Khakimov, S., Rakhmonov, A., Rajapova, S., & Rakhimbaev, Z. (2023). Traffic intensity on roads with big longitudinal slope in mountain conditions. E3S Web of Conferences, 401, 01073. https://doi.org/10.1051/e3sconf/202340101073

16. Ikromov, A. (2023). Components modifying methods with the using of energy technologies. 060037. https://doi.org/10.1063/5.0115559

17. Kasimov, O. (2023). Method for regulation of permissible irregularity of brake forces on front axle. E3S Web of Conferences, 401, 02033. https://doi.org/10.1051/e3sconf/202340102033

18. Kasimov, O., & Tukhtamishov, S. (2023). Mathematical model of braking process of car. E3S Web of Conferences, 401, 02034. https://doi.org/10.1051/e3sconf/202340102034

19. Keldiyarova, M., Ruzimov, S., Bonfitto, A., & Mukhitdinov, A. (2022). Comparison of two control strategies for range extender hybrid electric ve-hicles. 2022 International Symposium on Electromobility (ISEM), 1–6. https://doi.org/10.1109/ISEM55847.2022.9976663

20. Khakimov, S., Fayzullaev, E., Rakhmonov, A., & Samatov, R. (2021). Variation of reaction forces on the axles of the road train depending on road longitudinal slope. E3S Web of Conferences, 264, 05030. https://doi.org/10.1051/e3sconf/202126405030

21. Kulmukhamedov, Z., Khikmatov, R., Erbekov, S., & Saidumarov, A. (2022). Maximum temperature values of the engine and auto motor vehi-cles units in conditions of elevated ambient temperatures. 030040. https://doi.org/10.1063/5.0093466

22. Kulmukhamedov, Z., Khikmatov, R., Saidumarov, A., & Kulmukha-medova, Y. (2021). Theoretical research of the external temperature influ-ence on the traction and speed

properties and the fuel economy of cargo-carrying vehicles. Journal of Applied Engineering Science, 19(1), 68–76. https://doi.org/10.5937/jaes0-27851

23. Kutlimuratov, K., Khakimov, S., Mukhitdinov, A., & Samatov, R. (2021). Modelling traffic flow emissions at signalized intersection with PTV vissim. E3S Web of Conferences, 264, 02051. https://doi.org/10.1051/e3sconf/202126402051

24. Mavlonov, J., Ruzimov, S., Tonoli, A., Amati, N., & Mukhitdinov, A. (2023). Sensitivity Analysis of Electric Energy Consumption in Battery Electric Vehicles with Different Electric Motors. World Electric Vehicle Journal, 14(2), 36. https://doi.org/10.3390/wevj14020036

25. Mukhitdinov, A., Abdurazzokov, U., Ziyaev, K., & Makhmudov, G. (2023). Method for assessing the vehicle energy efficiency on a driving cy-cle. 060028. https://doi.org/10.1063/5.0114531

26. Mukhitdinov, A., Ziyaev, K., Abdurazzokov, U., & Omarov, J. (2023). Creation of the driving cycle of the city of Tashkent by the synthesis meth-od. 060029. https://doi.org/10.1063/5.0126363

27. Mukhitdinov, A., Ziyaev, K., Omarov, J., & Ismoilova, S. (2021). Meth-odology of constructing driving cycles by the synthesis. E3S Web of Con-ferences, 264, 01033. https://doi.org/10.1051/e3sconf/202126401033

28. Nurmetov, K., Riskulov, A., & Ikromov, A. (2022). Physicochemical as-pects of polymer composites technology with activated modifiers. 020011. https://doi.org/10.1063/5.0106358

29. Sanjarbek, R., Mavlonov, J., & Mukhitdinov, A. (2022). Analysis of the Powertrain Component Size of Electrified Vehicles Commercially Available on the Market. Communications - Scientific Letters of the University of Zilina, 24(1), B74–B86. https://doi.org/10.26552/com.C.2022.1.B74-B86

30. Topalidi, V., Yusupov, U., & Allaberganov, S. (2022). Improving the ef-ficiency of transport logistics support. 030072. https://doi.org/10.1063/5.0089587

31. Tursunov, S., & Khikmatov, R. (2023). Increasing environmental safety, increasing service life of ice units and assembly and saving fuel consump-tion through application of multifunctional fuel additives. E3S Web of Conferences, 365, 01012. https://doi.org/10.1051/e3sconf/202336501012

32. Usmanov, U., Ruzimov, S., Tonoli, A., & Mukhitdinov, A. (2023). Mod-eling, Simulation and Control Strategy Optimization of Fuel Cell Hybrid Electric Vehicle. Vehicles, 5(2), 464–481. https://doi.org/10.3390/vehicles5020026

33. Yusupov, U., Kasimov, O., & Anvarjonov, A. (2022). Research of the re-source of tires of rotary buses in career conditions. 030073. https://doi.org/10.1063/5.0089590

34. Yusupov, U., & Mukhitdinov, A. (2023). Evaluation of the influence of the longitudinal slope of carriage roads on the tire life. E3S Web of Confer-ences, 401, 03025. https://doi.org/10.1051/e3sconf/202340103025

35. Avdeychik, S., Goldade, V., Struk, V., Antonov, A., & Ikromov, A. (2020). THE PHENOMENON OF NANOSTATE IN MATERIAL SCIENCE OF FUNCTIONAL COMPOSITES BASED ON INDUSTRIAL POLYMERS. Theoretical & Applied Science, (7), 101-107.

TOSHKENT DAVLAT TRANSPORT UNIVERSITETI
Tashkent state transport university
International Journal Of Transport And Technological Machines
Tashkent 2024, issue 1, https://ijttm.uz/

STUDY OF PERFORMANCE INDICATORS OF EXCAVATORS

Zakir Maksudov[1 a)], Kamoliddin Rustamov[1, b)], Ziyovuddin Pardabaev[1,]
[1]*Tashkent State Transport University, Tashkent, Uzbekistan*
[a)]*z.makhsudov@mail.ru* [b)] *Corresponding author: k.j.rustamov82@gmail.com*

Abstract. The article presents a study of the indicators of the process of the appearance of failures of an excavator, operational indicators of the reliability of machines such as: the average number of failures, the parameter of the flow of failures and the time between failures and presents methods for determining these indicators. Based on the results of the study, the values of the excavator's time between failures were determined. The values of gamma-percentage resources limiting the reliability of parts and assemblies of the DOOSAN brand excavator have been established.

Keywords: reliability, failure, flow, parameter, process, operating time, average number of failures.

Introduction

High rates of construction of roads, as well as industrial and residential facilities, are ensured with the intensive and reliable operation of road-building machines. Therefore, increasing the efficiency of use and reliability of machines that meet the requirements of operation in various climatic zones, namely hot climate zones, is a very urgent problem for the Republic of Uzbekistan.

It is known that the reliability of machines manifests itself in the process of use and depends on the methods and operating conditions, the adopted system for its repair, maintenance methods, operating modes, as well as climatic operating conditions.

Based on this, the study of the reliability indicators of hydraulically driven single-bucket excavators operated in a hot climate zone is a particularly integral task of the study.

The problem of increasing the efficiency of road-building and specialized machines, especially those with hydraulic drive in hot climates, can currently be solved in two ways.

The first is the adaptation of the design of existing machines used in the conditions under consideration by equipping it with special equipment, which makes it possible to reduce the negative impact on the design of factors, adverse operating conditions of the hot climate zone.

This path is more accessible to operators, makes it possible to make fuller use of the potential of machine design, but by no means solves the problem under consideration as a whole and at the required technical level.

However, the existing huge fleet of road construction machines operating today in the hot climate zone still urgently requires the implementation of this path.

The purpose of developing management methods for technical operation, i.e. the processes of service maintenance and repairs of road-building machines with a hydraulic drive are to ensure the operability of the machines in operation. Operability - the state of road construction machines, in which the values of all parameters, including resource indicators of reliability, characterizing the performance of specified functions, meet the requirements of regulatory and technical and design documentation. [1, 3, 8, 24].

Materials and methods

The performance indicators of single-bucket excavators include: operating time T, average number of failures d_j, failure flow parameters λ_j, time to failure T_{nar}, gamma percentage (80 and 90%) resources of parts and assemblies, utilization factors K_i and technical use $K_{t.i.}$ and etc.

To determine the mean time to failure, it is necessary to have observational data during the period of operation or testing of the machine under specified conditions. Time to

failure is determined t_1, t_2, t_3, ……, t_n machines, and with the help of these operating hours, an indicator of the average operating time is obtained

$$T_{mid} = \frac{1}{N}\sum_{i=1}^{N} t_i \quad (1)$$

where t_i - operating time of parts and assemblies, hour;

N - number of machines.

In the case of the Weibull distribution

$$T_{mid} = aG\left(1+\frac{1}{b}\right) \quad (2)$$

Where a and b – constant distribution parameters;

G- gamma function sign;

and for the Rayleigh distribution

$$T_{mid} = a\frac{\sqrt{t_i}}{2} \quad (3)$$

For repaired parts (products for the period from operating time t_1 before running time t_2) time between failures is determined

$$T = \frac{t_2 - t_1}{H(t_2) - H(t_1)}, \quad (4)$$

or approximately:

$$T = \frac{t_2 - t_1}{m(t_2) - m(t_1)} \quad (5)$$

where $H(t_1)$ and $H(t_2)$ - respectively characterizes the flow of failures from the period of operation t_1 to operation t_2;

$m_{mid}(t_1)$ and $m_{mid}(t_2)$ - respectively, the average number of failures from the period of operation t_1 to operation t_2.

After some work T_o function $H(T)$, characterizing the flow of failures becomes linear and takes the form

$$H(T)=H(T_o)+\omega(T-T_o), \quad (6)$$

where ω=const. Period $T=T_o$ called the run-in period; $\omega=T$, characterizing the failure flow parameter is determined by the equation

$$\omega(T) = \frac{dH(T)}{dT}, \quad (7)$$

or approximately

$$\omega(T) = \frac{\sum_{i=1}^{N} mi(T+\Delta T) - \sum_{i=1}^{N} mi(T)}{N\Delta T} \quad (8)$$

where N- number of monitored machines;

ΔT – a fairly short period of time;

m_i - the number of failures for each product (machines, mechanism and parts). [1, 6, 10, 23]

Further, approaches and other ways are presented for determining the reliability indicators of the investigated single-bucket excavators with a hydraulic drive using machines in a certain period of operation, the purpose of determining the reliability indicators of the studied machines, assessing their functioning in a hot climate zone, determining the influence of operating conditions factors on the efficiency and reliability of machines. In this case, for single-bucket excavators with a hydraulic drive of the DOOSAN brand in the operating conditions of a hot climate zone.

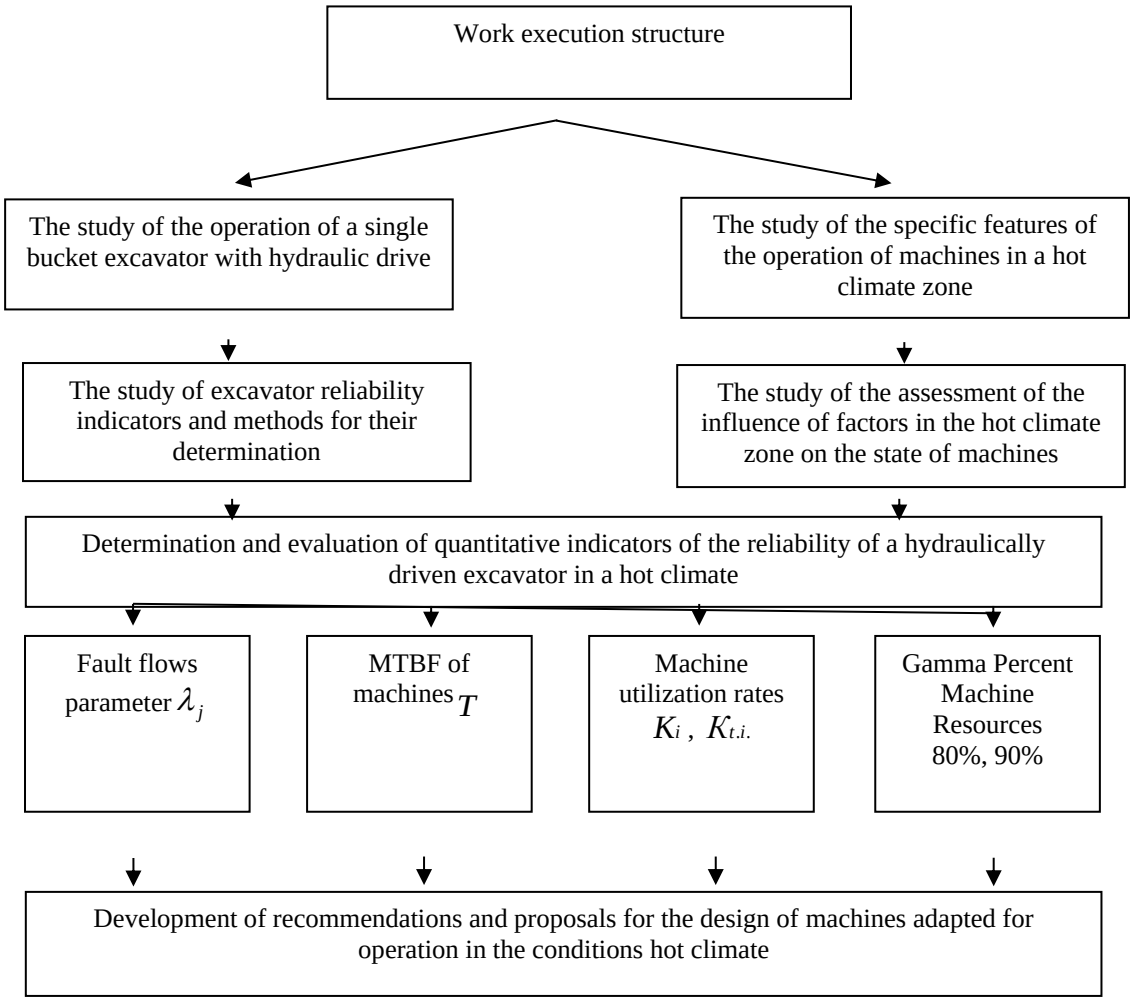


Fig.1. The structure of the study to determine the performance indicators of the reliability of excavators.

The average number of failures per one surveyed machine in *i*-operating time interval (T_{nar}), was determined by the formula

$$d_j = \frac{m_j}{N_j} \quad (9)$$

where m_j - the number of failurees for all machines in a given interval;
N_j - the num 4
7 ber of machines observed in this interval.
The time between failures for the observation period was determined by the formula

$$T = \frac{T_{nar}}{\sum dj} \quad (10)$$

where T_{nar} - operating time for the observation period, moto-hour;
$\sum d_j$ - total average number of failures.
The failure flow parameter is determined by the formula

$$\lambda = \frac{d_j}{\Delta j} \quad (11)$$

where Δj - operating intervals of controlled machines;

d_j - average number of failures per machine.

Increasing the working capacity offers an increase in the proportion of time that road construction machines are in working condition. Therefore, an indicator of the measure of achieving the goal can be the coefficient of technical use $K_{T.I.}$.

Achieving the goal is ensured by reducing the number of unscheduled repairs, i.e. operational repairs in excess of standard service downtime and repairs, downtime due to untimely delivery of spare parts. [1, 2, 14, 23]

The structure of the study to determine the operational reliability indicators of excavators is shown in fig. one.

The algorithm block diagram for determining the performance indicators of the reliability of the excavator is shown in fig. 2.

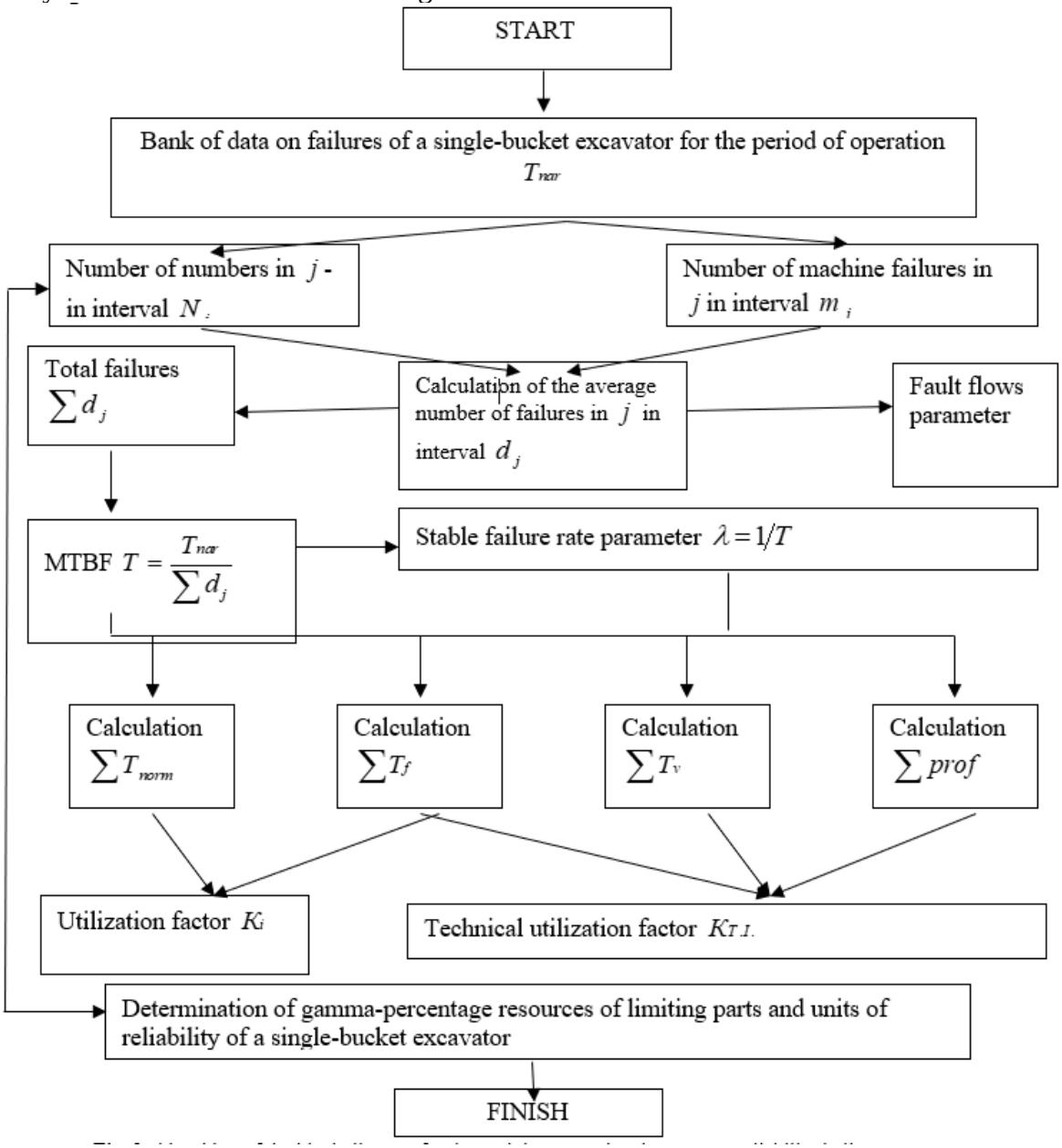


Fig. 2. Algorithm of the block diagram for determining operational excavator reliability indicators

Management of the processes of maintenance and repair of road-building machines, as well as the technical condition of hydraulically driven road-building machines is aimed at increasing the level of their reliability in operation. It includes control and accounting of the technical condition of road construction machines, units and assemblies optimal planning and organization of maintenance and repair based on predicting changes in the technical condition, as well as through operational reliability indicators such as MTBF (T_{nar}), bounce flow parameter (λ_i) and gamma-percentage resources of parts and assemblies.

Results and Discussion

Further, according to the methodology, performance indicators are calculated that characterize the resource values of the use of machines. The average number of failures per machine in the th interval is determined by formula (9), the failure rate parameter by formula (11), and the time between failures by formula (10) and the results are presented in Table 1. [4, 9, 20]

The results of calculating the values of the parameters of the failure flows (λ_j), for j - that intervals of an operating time. Calculation of the average number of failures per machine in j - that operating time interval is made according to the formula (9).

$$d_{j1} = m_{j1} / N_{j1} = 11 / 5 = 2,2$$
$$d_{j\,2} = m_{j2} / N_{j2} = 8 / 6 = 1,33$$
$$d_{j3} = m_{j3} / N_{j3} = 7 / 4 = 1,75$$

and the calculation of the failure rate parameter in j - that interval of operating time was carried out according to the formula (11)

$$\lambda_{j1} = d_{j1} / \triangle_{j1} = 2,2 / 250 = 0,0088$$
$$\lambda_{j2} = d_{j2} / \triangle_{j2} = 1,33 / 250 = 0,0053$$
$$\lambda_{j3} = d_{j3} / \triangle_{j3} = 1,75 / 250 = 0,0070$$

the values of d_{jn} and λ_{jn} were calculated in a similar way, and the calculation results are summarized in Table 1.

Planning of operational repairs, considering the working capital of units and assembly units, as well as the availability of posts for the repair of a particular enterprise, in order to reduce abnormal downtime of machines in case of failure. The failure rate parameter of the DOOSAN shovel excavator is presented in Table 1.

Table 1. Failure flow parameter of the excavator

No	Operating intervals	The number of cars observed in this interval N_j	The number of machine failures in a given interval m_j	Average number of failures per machine d_j	Fault flow parameter λ_j
1	0-250	5	11	2,20	0,0088
2	251-500	6	8	1,33	0, 0053
3	501-750	4	7	1,75	0,0070
4	751-1000	5	7	1,40	0,0056
5	1001-1250	3	4	1,33	0,0053
6	1251-1500	3	5	1,67	0,0066
7	1501-1750	5	6	1,20	0,0048
8	1751-2000	5	8	1,60	0,0064
9	2001-2250	6	9	1,50	0,0060
10	2251-2500	4	7	2,75	0,0070

11	2501-2750	5	8	1,60	0,0064
12	2751-3000	6	8	1,33	0,0053
13	3001-3250	4	7	1,75	0,0070
14	3251-3500	5	10	2,00	0,0080

Next, let's build a graph of the relationship between λ_j, and T of the failure rate parameter of a single-bucket excavator of the DOOSAN brand. The graph of the dependence between λ_j of the failure rate parameter and T operating time of the DOOSAN excavator is shown in fig. one.

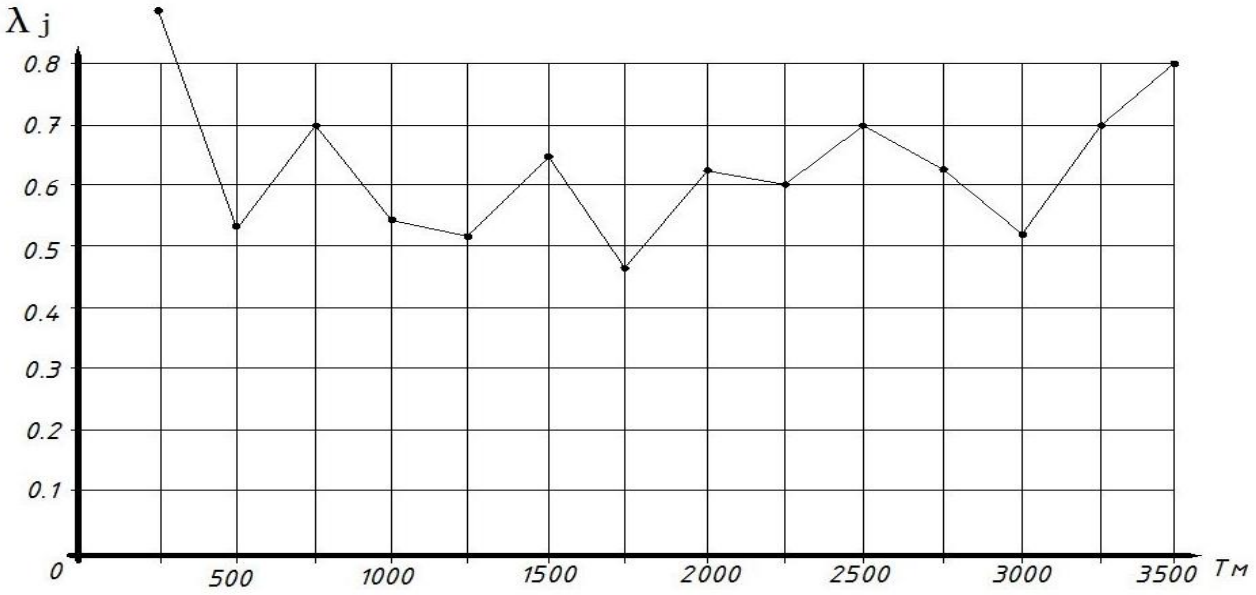


Fig. 3. Dependences of the failure rate parameter λ_j and the operating time of the DOOSAN brand excavator; $T_{p90} = 1092h$ $T_{p80} = 1816h$

Based on the obtained failure rate parameters, the value of the time between failures of the studied single-bucket excavator of the DOOSAN brand was determined. The time between failures T of the investigated single-bucket excavator with a hydraulic drive of the DOOSAN brand was determined according to the formula (10)

$T = T_{nar} / \sum d_j = 3500 / 21,46 = 163,1$ hour/failure.

As can be seen from Fig. 1. The initial period of operation of excavators with an operating time of up to 750 motor-hours is characterized by an increase in the failure rate. This is primarily due to the fact that during the initial period of operation, the parts of the machine are running in and some types of technological defects appear, sometimes referred to as factory failures of machines.

The second period of operation from 750 to 3000 hours is characterized by normal operating conditions of the machines, i.e. stable operation. Because, during this period of operation, the value of the failure flow parameter stabilizes, and fluctuates around the values:

$\lambda' = 1 / T = 1 / 163,1 = 0,0061$.

The third period of operation of the machines begins with the operating time of 3250 motor-hours. During this period of operation, the value of the failure rate parameter tends to

increase and is explained by an increase in the wear of parts of the DOOSAN shovel excavator.

When determining the average number of failures per machine in the j - that interval of operating time, the obtained data presented in Table 1 was used to clarify the number of machines Nj that came across in the j - that interval.

The results of the study: the parameter of failure flows, time between failures and in general for machines, as well as average resources or average time intervals are used to solve practical problems in the operation of machines, namely, when predicting and determining the need to replace parts, assembly units, units for the planned period for the fleet of machines or planning the production of spare parts.

Planning for operational repairs, considering the working capital of units and assembly units, as well as the availability of posts for the repair of a particular enterprise, in order to reduce abnormal downtime of machines in case of failure. [12,15,18,21]

The failure rate parameter of the DOOSAN shovel excavator is presented in Table 1.

Further, we consider methods and determination of resource indicators of parts and units of limiting reliability of machines, using the example of a single-bucket excavator of the DOOSAN brand.

It is known that certain values of resource indicators of parts and assemblies of machines make it possible to justify the time, frequency and need for maintenance of machines, and can also be the basis for the development of technical specifications on the need for operational repairs.

The established resource indicators of parts, components and assemblies of machines allow the rational organization and conduct of current repairs of machines, and these indicators can fully replace the frequency of current repairs of specific components and assemblies, as well as quickly wearing parts and their assemblies.

Next, we consider the theoretical and methodological foundations for determining the resource indicators of parts and machine assemblies. Calculation of the ordinate of the empirical resource distribution function of the part and assemblies. [5, 7, 11, 22]

In this paper, we consider the definition of resource indicators for parts and assemblies of single-bucket excavators of the DOOSAN brand as an example, which allows you to set the time for current repairs, as well as the replacement of wear parts in operating conditions, which are the result of a gradual failure of machines.

We calculate the resource indicators of the cuff 90 x 110 of the hydraulic cylinder of the boom of a single-bucket excavator of the DOOSAN brand. The increment of the first resource value is calculated according to the formula (13):

$$\Delta_1 = \frac{N+1-m_{i-1}}{N+1-N_i} = \frac{20+1-0}{20+1-1} = 1{,}05$$

The serial number of the first resource value is determined by the formula (14)

$$m_1 = m_{i-1} + \Delta_i = 0 + 1{,}05 = 1{,}05$$

Next, we determine the first orbit of the empirical function by the formula (15)

$$\mathrm{F}_{э_1} = \frac{m_i}{N+1} = \frac{1{,}05}{20+1} = 0{,}05$$

Thus, we calculate similarly for the increment of the second resource value $\Delta_i = \Delta_2$, under $N_i = 2$.

$$\Delta_2 = \frac{N+1-m_{i-1}}{N+1-N_i} = \frac{20+1-1{,}05}{20+1-2} = 1{,}05$$

And the ordinal number of the second resource value is equal to

$m_2 = m_{i-1} + \Delta_2 = 1{,}05 + 1{,}05 = 2{,}1$

The ordinate of the empirical function of the second resource value is

$$F_{э_2} = \frac{m_2}{N+1} = \frac{2{,}1}{21} = 0{,}1$$

Next, we calculate the increment of the fourth resource value $\Delta_i = \Delta_4$.

$$\Delta_4 = \frac{N+1-m_i}{N+1-N_i} = \frac{20+1-2{,}1}{20+1-4} = 1{,}11$$

Then the ordinal number of the resource value is equal to

$m_4 = m_2 + \Delta_4 = 2{,}1 + 1{,}11 = 3{,}21$

And the ordinate of the empirical function is

$$F_{ei} = \frac{m_4}{N+1} = \frac{3{,}21}{21} = 0{,}15$$

Calculation of the increment of the sixth resource value, $\Delta_i = \Delta_6$

$$\Delta_6 = \frac{N+1-m_i}{N+1-N_1} = \frac{20+1-3{,}21}{20+1-6} = 1{,}19$$

Then the ordinal number of the resource value is equal to

$m_6 = m_4 + \Delta_6 = 3{,}21 + 1{,}19 = 4{,}40$

And the ordinate of the empirical function is

$$F_{э6} = \frac{m_6}{N+1} = \frac{4{,}4}{20+1} = 0{,}21$$

Further, the subsequent increments of the resource values are calculated in a similar way, and the results of the calculations are listed in the table 2.

Based on the results of the calculation presented in Table 2, we construct the graphical ordinate of the empirical function between $F_{ei} - T_{nar}$ to determine the 80% and 90% resource of the cuff 90 x 110 of the hydraulic cylinder of the boom of the DOOSAN excavator, which is presented in fig. 4.

Table 2. Calculation of the ordinate of the empirical resource distribution function of the cuff 90 x 110 excavator brand "DOOSAN"

№	MTBF $T_н$	Number of stopped running hours r_i	Number of suspended running hours n_i	Number of machines stops N_i	Number of machines $N+1-m_{i-1}$ $N+1-N_i$		Resource value increments Δ_i	Sequence number of the resource value m_i	Empirical function ordinate $F_{э_i}$
1	377		1	1	21	20	1,05	1,05	0,05
2	404	1							
3	422		1	2	19,95	19	1,05	2,1	0,10
4	457	1							
5	481		1	4	18,9	17	1,11	3,21	0,15
6	487	1							
7	585		1	6	17,79	15	1,19	4,40	0,21

8	652		1				1,19	5,59	0,27
9	711		1				1,19	6,78	0,32
10	758	1							
11	825		1	10	4,22	11	1,29	8,07	0,38
12	859		1						
13	917	1					1,29	9,36	0,45
14	986		1	13	11,64	8	1,46	10,82	0,52
15	1086		1				1,46	12,28	0,58
16	1172		1				1,46	13,74	0,65
17	1261	1							
18	1414		1	18		3	2,42	16,16	0,77
19	1473	1							

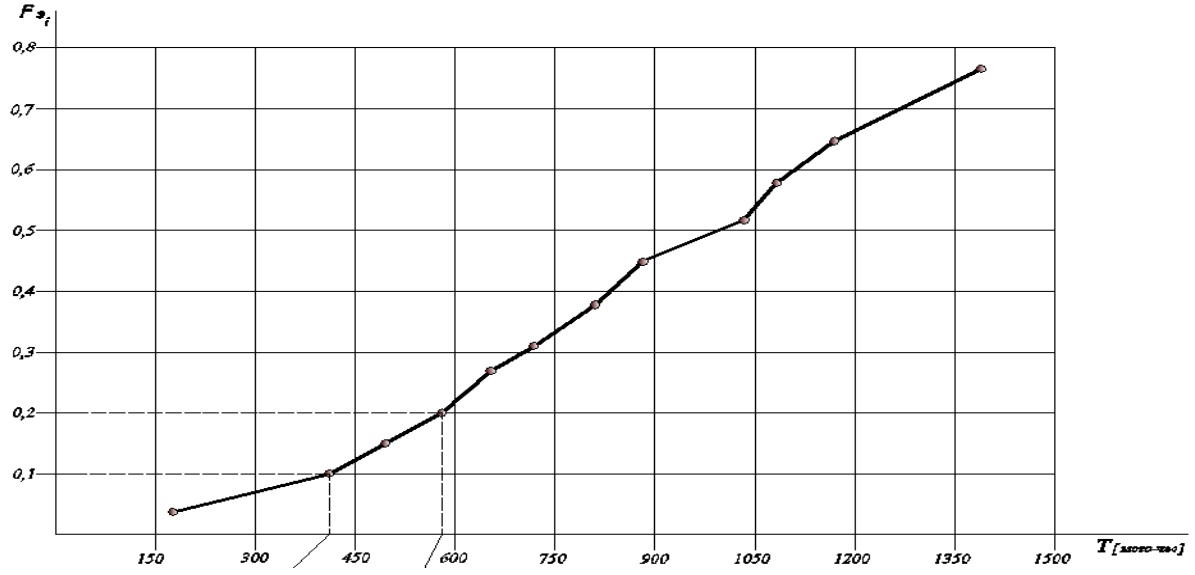


Fig. 4. Determination of 80% and 90% resource cuff 90x110 hydraulic cylinder excavator brand "DOOSAN";

$$T_{p90} = 768h \;\; T_{p80} = 1322h$$

From the constructed graph of functions fig. 2. it can be seen that 80% and 90% of the resource of the cuff 90 x 110 of the hydraulic cylinder of the excavator boom is $T_{p80} = 580{,}0$ moto-hour, and 90% resource is equal to $T_{p90} = 422{,}0$ moto hour.

Thus, these established resource indicators for the cuff of the hydraulic cylinder of the excavator boom can fully replace the frequency of the current repair of hydraulic cylinders to replace the worn-out set of seals. [18,19,24].

Conclusion

According to the results of the research, we can draw the following conclusions: The parameter of the failure rate of the DOOSAN brand shovel excavator has been determined and justified. The regularity of the distribution of the failure flow parameters of the single-bucket excavator of the brand "DOOSAN" was studied and determined. The values of

gamma-percentage resources limiting the reliability of parts and assemblies of a single-bucket excavator of the DOOSAN brand were determined and substantiated, namely:

- gamma-percentage (80% and 90%) cuff resources 90 x 110 of the hydraulic cylinder of the excavator boom, which are equal, respectively $T_{p80} = 580{,}0$ moto hour and $T_{p90} = 422{,}0$ moto hour;
- gamma-percentage (80% and 90%) resources of the cross of the connection of the bridges of the excavator, which are equal, respectively $T_{p80} = 1816{,}0$ moto hour and $T_{p90} = 1092$ moto hour;
- gamma-percentage (80% and 90%) resources of the excavator working equipment ring, which are equal, respectively $T_{p80} = 1322{,}0$ moto hour and $T_{p90} = 768{,}0$ moto hour.

The developed method for determining the gamma-percentage resources of parts and units of limiting reliability of machines allows planning the consumption of spare parts (parts and units) of the DOOSAN brand excavator.

References

1. Sheinin, A.M. etc., (1992). Operation of road machines. M.: Transport.
2. Volkov, D.P., Nikolaev, S.N., (1989). Reliability of construction machines and equipment. Moscow: Higher school.
3. Maloletkov, E.K., (1988). Reliability and durability of building and road machines. M.: TsNIIOMTP.
4. Methodology for predicting the reliability indicators of construction and road machines at the design stage, (1988). Moscow: VNIIStroydormash.
5. "Construction and road building machinery", (2019). MOSCOW, (2, 6, 9).
6. Guidelines for the collection and processing of information on the reliability of machines and equipment MU-29-12-95, (1995). Moscow.
7. Askarhodzhaev, T., Maksudov Z., (2012). Industry norms of labor and mechanized costs of modern mechanisms and equipment in the construction, repair and maintenance of highways. *Departmental building codes*. VSN 62-11. Tashkent, p. 180.
8. Askarhodzhaev, T., Maksudov, Z., (2013). Requirements of road equipment for routine repair and maintenance of highways, *Departmental rules and regulations*, MKN 36-2008, p. 96. Tashkent
9. Maksudov, Z.T., Khankelov, T.K., Yusupova, N.Z., (2019). Formation of a rational set of cars based on the developed standard labor intensity for the construction and repair of highways, *Belarusian State University of Transport.* pp. 157-161, Gomel.
10. Askarhodzhaev, T.I., Maksudov, Z.T., (2011) Operation of road-building machines, *A textbook for university students*, p. 324, Tashkent.
11. Maksudov, Z.T, Kudaybergenov, M, Ismailov, J., (2019). On the frequency of service maintenance of the "SHANTUI SD 32" bulldozer in terms of fuel consumption and machine production, *Collection of scientific papers of the eighth international scientific-practical conference*, pp.151-154 , Almaty.
12. Methods for static processing of information on the reliability of construction and road machines, (1997). RTM 22342-97, M.,
13. Khankelov, T., Tursunov, S.H., Maksudov Z., (2020). Domestic Solid Waste Crusher, *International Journal of Psychological Rehabilitation, 24*(07), 8090-8091.
14. Grinevich G.P. etc., (1991). Reliability of building machines. Moscow: Stroyizdat.

15. News from road machinery DOOSAN, KOREY.
16. Internet www. Technic service, road machinery. EXKAVATOR. RU.
17. Internet www. Technic service, hydraulic EXSKAVATOR. RU.
18. Internet www. Technic servis, HYDRAVLIC EXSKAVATOR, KOREY.
19. PATENT. ENGLAHD, F2B, "Weston" Co. Ltd.
20. Balovnev, V.I. etc. (2001). Building machines and complexes. Moscow, Mashinostroenie.
21. Internet www.Technic service, HYDRAVLIC EXSKAVATOR. RU.
22. Balovnev, V.I. etc., (2001). Building machines and complexes. Moscow, Mashinostroenie.
23. Khazov, B.F., (1986). Handbook for calculating the reliability of machines at the design stage. Moscow, Mashinostroenie,
24. Sheinin, A.M., (1987). Patterns of the influence of the reliability of machines on the efficiency of their operation. Moscow: Knowledge.